# 12

# ELECTRODYNAMIC FIELDS: THE SUPERPOSITION INTEGRAL POINT OF VIEW

## 12.0 INTRODUCTION

This chapter and the remaining chapters are concerned with the combined effects of the magnetic induction $\partial\mathbf{B}/\partial t$ in Faraday's law and the electric displacement current $\partial\mathbf{D}/\partial t$ in Ampère's law. Thus, the full Maxwell's equations without the quasistatic approximations form our point of departure. In the order introduced in Chaps. 1 and 2, but now including polarization and magnetization, these are, as generalized in Chaps. 6 and 9,

$$\nabla \cdot (\epsilon_o \mathbf{E}) = \rho_u - \nabla \cdot \mathbf{P} \tag{1}$$

$$\nabla \times \mathbf{H} = \mathbf{J}_u + \frac{\partial}{\partial t}(\epsilon_o \mathbf{E} + \mathbf{P}) \tag{2}$$

$$\nabla \times \mathbf{E} = -\frac{\partial}{\partial t}\mu_o(\mathbf{H} + \mathbf{M}) \tag{3}$$

$$\nabla \cdot (\mu_o \mathbf{H}) = -\nabla \cdot (\mu_o \mathbf{M}) \tag{4}$$

One may question whether a generalization carried out within the formalism of electroquasistatics and magnetoquasistatics is adequate to be included in the full dynamic Maxwell's equations, and some remarks are in order. Gauss' law for the electric field was modified to include charge that accumulates in the polarization process. The accounting for the charge leaving a designated volume was done under no restrictions of quasistatics, and thus (1) can be adopted in the fully dynamic case. Subsequently, Ampère's law was modified to preserve the divergence-free character of the right-hand side. But there was more involved in that step. The term $\partial\mathbf{P}/\partial t$ can be identified unequivocally as the current density associated with a time dependent polarization process, provided that the medium as a whole is at rest. Thus, (2) is the correct generalization of Ampère's law for polarizable media

at rest. If the medium moves with the velocity $\mathbf{v}$, a term $\nabla \times (\mathbf{P} \times \mathbf{v})$ has to be added to the right-hand side[1,2]. The generalization of Gauss' law and Faraday's law for magnetic fields is by analogy. If the material is moving and magnetized, a term $-\mu_o \nabla \times (\mathbf{M} \times \mathbf{v})$ must be added to the right-hand side of (3). We shall not consider such moving polarized or magnetized media in the sequel.

Throughout this chapter, we are generally interested in electromagnetic fields in free space. If the region of interest is filled by a material having an appreciable polarization and or magnetization, the constitutive laws are presumed to represent a linear and isotropic material

$$\mathbf{D} \equiv \epsilon_o \mathbf{E} + \mathbf{P} = \epsilon \mathbf{E} \tag{5}$$

$$\mathbf{B} \equiv \mu_o (\mathbf{H} + \mathbf{M}) = \mu \mathbf{H} \tag{6}$$

and $\epsilon$ and $\mu$ are assumed uniform throughout the region of interest.[1] Maxwell's equations in linear and isotropic media may be rewritten more simply

$$\nabla \cdot \epsilon \mathbf{E} = \rho_u \tag{7}$$

$$\nabla \times \mathbf{H} = \mathbf{J}_u + \frac{\partial}{\partial t} \epsilon \mathbf{E} \tag{8}$$

$$\nabla \times \mathbf{E} = -\frac{\partial}{\partial t} \mu \mathbf{H} \tag{9}$$

$$\nabla \cdot \mu \mathbf{H} = 0 \tag{10}$$

Our approach in this chapter is a continuation of the one used before. By expressing the fields in terms of superposition integrals, we emphasize the relationship between electrodynamic fields and their sources. Next we take into account the effect of conducting bodies upon the electromagnetic field, introducing the boundary value approach.

We began Chaps. 4 and 8 by expressing an irrotational $\mathbf{E}$ in terms of a scalar potential $\Phi$ and a solenoidal $\mathbf{B}$ in terms of a vector potential $\mathbf{A}$. We start this chapter in Sec. 12.1 with the generalization of these potentials to represent the electric and magnetic fields under electrodynamic conditions. Poisson's equation related $\Phi$ to its source in Chap. 4 and $\mathbf{A}$ to the current density $\mathbf{J}$ in Chap. 8. What equation relates these potentials to their sources when quasistatic approximations do not apply? In Sec. 12.1, we develop the inhomogeneous wave equation, which assumes the role played by Poisson's equation in the quasistatic cases. It follows from this equation that for linearly polarizable and magnetizable materials, the superposition principle applies to electrodynamics.

The fields associated with source singularities are the next topic, in analogy either with Chaps. 4 or 8. In Sec. 12.2, we start with the field of an elemental charge and build up the field of a dynamic electric dipole. Here we exemplify the launching of an electromagnetic wave and see how the quasistatic electric dipole fields relate to the more general electrodynamic fields. The section concludes by deriving the electrodynamic fields associated with a magnetic dipole from the fields

[1] To make any relation in this chapter apply to free space, let $\epsilon = \epsilon_o$ and $\mu = \mu_o$.

for an electric dipole by exploiting the symmetry of Maxwell's equations in source-free regions.

The superposition integrals developed in Sec. 12.3 provide particular solutions to the inhomogeneous wave equations, just as those of Chaps. 4 and 8, respectively, gave solutions to the scalar and vector Poisson's equations. In describing the operation of antennae, the fields that radiate away from the source are of primary interest. The superposition integrals for these radiation fields are used to find antenna radiation patterns in Sec. 12.4. The discussion of antennae is continued in Sec. 12.5, which has as a theme the complex form of Poynting's theorem. This theorem makes it possible to model the impedance of antennae as "seen" by their driving sources.

In Sec. 12.6, the field sources take the form of surface currents and surface charges. It is generally not convenient to find the associated fields by making direct use of the superposition integrals. Nevertheless, the sources are a "given," and any method that results in the associated fields amounts to solving the superposition integrals. This section provides a first view of the solutions to the wave equation in Cartesian coordinates that will be derived from the boundary value point of view in Chap. 13. In preparation for the boundary value approach of the next chapter, boundary conditions are satisfied by appropriate choices of sources. Thus, the parallel plate waveguide considered from the boundary value point of view in Chap. 13 is seen here from the point of view of waves initiated by given sources. The method of images, taken up in Sec. 12.7, provides further examples of this approach to satisfying boundary conditions.

When boundaries are introduced in this chapter, they are presumed to be perfectly conducting. In Chap. 13, the boundaries can also be interfaces between perfectly insulating dielectrics. In both of these chapters, the theme is dynamical phenomena related to the propagation and reflection of electromagnetic waves. The dynamics are characterized by one or more electromagnetic transit times, $\tau_{em}$. Dynamical phenomena associated with charge relaxation or magnetic diffusion, characterized by $\tau_e$ and $\tau_m$, are excluded. We will look at these again in Chaps. 14 and 15.

## 12.1 ELECTRODYNAMIC FIELDS AND POTENTIALS

In this section, we extend the use of the scalar and vector potentials to the description of electrodynamic fields. In regions of interest, the current density $\mathbf{J}$ of unpaired charge and the charge density $\rho_u$ are prescribed functions of space and time. If there is any material present, it is of uniform permittivity $\epsilon$ and permeability $\mu$, $\mathbf{D} = \epsilon\mathbf{E}$ and $\mathbf{B} = \mu\mathbf{H}$. For quasistatic fields in such regions, the potentials $\Phi$ and $\mathbf{A}$ are governed by Poisson's equation. In this section, we see the role of Poisson's equation for quasistatic fields taken over by the inhomogeneous wave equation for electrodynamic fields.

In both Chaps. 4 and 8, potentials were introduced so as to satisfy automatically the one of the two laws that was source free. In Chap. 4, we made $\mathbf{E} = -\nabla\Phi$ so that $\mathbf{E}$ was automatically irrotational, $\nabla \times \mathbf{E} = 0$. In Chap. 8 we let $\mathbf{B} = \nabla \times \mathbf{A}$ so that $\mathbf{B}$ was automatically solenoidal, $\nabla \cdot \mathbf{B} = 0$. Of the four laws comprising Maxwell's equations, (12.0.7)–(12.0.10), those of Gauss and Ampère involve

sources, while the last two, Faraday's law and the magnetic flux continuity law, do not. Following the approach used before, potentials should be introduced that automatically satisfy Faraday's law and the magnetic flux continuity law, (12.0.9) and (12.0.10). This is the objective of the following steps.

Given that the magnetic flux density remains solenoidal, the vector potential **A** can be defined just as it was in Chap. 8.

$$\boxed{\mathbf{B} = \mu\mathbf{H} = \nabla \times \mathbf{A}} \tag{1}$$

With $\mu\mathbf{H}$ represented in this way, (12.0.10) is again automatically satisfied and Faraday's law, (12.0.9), becomes

$$\nabla \times \big(\mathbf{E} + \frac{\partial \mathbf{A}}{\partial t}\big) = 0 \tag{2}$$

This expression is also automatically satisfied if we make the quantity in brackets equal to $-\nabla\Phi$.

$$\boxed{\mathbf{E} = -\nabla\Phi - \frac{\partial \mathbf{A}}{\partial t}} \tag{3}$$

With **H** and **E** defined in terms of $\Phi$ and **A** as given by (1) and (3), the last two of the four Maxwell's equations, (12.0.9–12.0.10), are automatically satisfied. Note, however, that the potentials that represent given fields **H** and **E** are not fully specified by (1) and (3). We can add to **A** the gradient of any scalar function, thus changing both **A** and $\Phi$ without affecting **H** or **E**. A further specification of the potentials will therefore be given shortly.

We now turn to finding the equations that **A** and $\Phi$ must obey if the laws of Gauss and Ampère, the first two of (12.0.9-12.0.10), are to be satisfied. Substitution of (1) and (3) into Ampère's law, (12.0.8), gives

$$\nabla \times (\nabla \times \mathbf{A}) = \mu\epsilon \frac{\partial}{\partial t}\big(-\nabla\Phi - \frac{\partial \mathbf{A}}{\partial t}\big) + \mu\mathbf{J}_u \tag{4}$$

A vector identity makes it possible to rewrite the left-hand side so that this equation is

$$\nabla(\nabla \cdot \mathbf{A}) - \nabla^2\mathbf{A} = \mu\epsilon \frac{\partial}{\partial t}\big(-\nabla\Phi - \frac{\partial \mathbf{A}}{\partial t}\big) + \mu\mathbf{J}_u \tag{5}$$

With the gradient and time derivative operators interchanged, this expression is

$$\nabla\big(\nabla \cdot \mathbf{A} + \mu\epsilon\frac{\partial \Phi}{\partial t}\big) - \nabla^2\mathbf{A} = -\mu\epsilon\frac{\partial^2 \mathbf{A}}{\partial t^2} + \mu\mathbf{J}_u \tag{6}$$

To uniquely specify **A**, we must not only stipulate its curl, but give its divergence as well. This point was made in Sec. 8.0. In Sec. 8.1, where we were concerned with MQS fields, we found it convenient to make **A** solenoidal. Here,

where we have kept the displacement current, we set the divergence of $\mathbf{A}$ so that the term in brackets on the left is zero.

$$\boxed{\nabla \cdot \mathbf{A} = -\mu\epsilon \frac{\partial \Phi}{\partial t}} \tag{7}$$

This choice of $\nabla \cdot \mathbf{A}$ is called the choice of the *Lorentz gauge*. In this gauge, the expression representing Ampère's law, (6), reduces to one involving $\mathbf{A}$ alone, to the exclusion of $\Phi$.

$$\boxed{\nabla^2 \mathbf{A} - \mu\epsilon \frac{\partial^2 \mathbf{A}}{\partial t^2} = -\mu \mathbf{J}_u} \tag{8}$$

The last of Maxwell's equations, Gauss' law, is satisfied by making $\Phi$ obey the differential equation that results from the substitution of (3) into (12.0.7).

$$\nabla \cdot \epsilon\Big( -\nabla\Phi - \frac{\partial \mathbf{A}}{\partial t}\Big) = \rho_u \Rightarrow \nabla^2 \Phi + \frac{\partial}{\partial t}(\nabla \cdot \mathbf{A}) = -\frac{\rho_u}{\epsilon} \tag{9}$$

We can substitute for $\nabla \cdot \mathbf{A}$ using (7), thus eliminating $\mathbf{A}$ from this expression.

$$\boxed{\nabla^2 \Phi - \mu\epsilon \frac{\partial^2 \Phi}{\partial t^2} = -\frac{\rho_u}{\epsilon}} \tag{10}$$

In summary, with $\mathbf{H}$ and $\mathbf{E}$ defined in terms of the vector potential $\mathbf{A}$ and scalar potential $\Phi$ by (1) and (3), the distributions of these potentials are governed by the *vector and scalar inhomogeneous wave equations* (8) and (10), respectively. The *unpaired* charge density and the *unpaired* current density are the "sources" in these equations. In representing the fields in terms of the potentials, it is understood that the "gauge" of $\mathbf{A}$ has been set so that $\mathbf{A}$ and $\Phi$ are related by (7).

The time derivatives in (8) and (10) are the result of retaining both the displacement current and the magnetic induction. Thus, in the quasistatic limits, these terms are neglected and we return to vector and scalar potentials governed by Poisson's equation.

**Superposition Principle.** The inhomogeneous wave equations satisfied by $\mathbf{A}$ and $\Phi$ [(8) and (10)] as well as the gauge condition, (7), are linear when the sources on the right are prescribed. That is, if solutions $\mathbf{A_a}$ and $\Phi_a$ are associated with sources $\mathbf{J}_a$ and $\rho_a$,

$$(\mathbf{J}_a,\ \rho_a) \Rightarrow (\mathbf{A}_a,\ \Phi_a) \tag{11}$$

and similarly, $\mathbf{J}_b$ and $\rho_b$ produce the potentials $\mathbf{A}_b$, $\Phi_b$,

$$(\mathbf{J}_b,\ \rho_b) \Rightarrow (\mathbf{A}_b,\ \Phi_b) \tag{12}$$

then the potentials resulting from the sum of the sources is the sum of the potentials.

$$[(\mathbf{J}_a + \mathbf{J}_b),\ (\rho_a + \rho_b)] \Rightarrow [(\mathbf{A}_a + \mathbf{A}_b),\ (\Phi_a + \Phi_b)] \tag{13}$$

The formal proof of this superposition principle follows from the same reasoning used for Poisson's equation in Sec. 4.3.

In prescribing the charge and current density on the right in (8) and (10), it should be remembered that these sources are related by the law of charge conservation. Thus, although $\Phi$ and $\mathbf{A}$ appear in (8) and (10) to be independent, they are actually coupled. This interdependence of the sources is reflected in the link between the scalar and vector potentials established by the gauge condition of (7). Once $\mathbf{A}$ has been found, it is often convenient to use this relation to determine $\Phi$.

**Continuity Conditions.** Each of Maxwell's equations, (12.0.7)–(12.0.10), as well as the charge conservation law obtained by combining the divergence of Ampère's laws with Gauss' law, implies a continuity condition. In the absence of polarization and magnetization, these conditions were derived from the integral laws in Chap. 1. Generalized to include polarization and magnetization in Chaps. 6 and 9, the continuity conditions for (12.0.7)–(12.0.10) are, respectively,

$$\mathbf{n} \cdot (\epsilon_a \mathbf{E}^a - \epsilon_b \mathbf{E}^b) = \sigma_{su} \tag{14}$$

$$\mathbf{n} \times (\mathbf{H}^a - \mathbf{H}^b) = \mathbf{K}_u \tag{15}$$

$$\mathbf{n} \times (\mathbf{E}^a - \mathbf{E}^b) = 0 \tag{16}$$

$$\mathbf{n} \cdot (\mu_a \mathbf{H}^a - \mu_b \mathbf{H}^b) = 0 \tag{17}$$

The derivation of these conditions is the same as given at the end of the sections introducing the respective integral laws in Chap. 1, except that $\mu_o \mathbf{H}$ is replaced by $\mu \mathbf{H}$ in Faraday's law and $\epsilon_o \mathbf{E}$ by $\epsilon \mathbf{E}$ in Ampère's law.

In Secs. 12.6 and 12.7, and in the following chapters, these conditions are used to relate electrodynamic fields to surface currents and surface charges. At the outset, we recognize that two of these continuity conditions are, like Faraday's law and the law of magnetic flux continuity, not independent of each other. Further, just as the laws of Ampère and Gauss imply the charge conservation relation between $\mathbf{J}_u$ and $\rho_u$, the continuity conditions associated with these laws imply the charge conservation continuity condition obeyed by the surface currents and surface charge densities.

To see the first interdependence, Faraday's law is integrated over a surface $S$ enclosed by a contour $C$ *lying in the plane of the interface*, as shown in Fig. 12.1.1a. Stokes' theorem is then used to write

$$\oint_C \mathbf{E} \cdot d\mathbf{s} = -\frac{d}{dt} \int_S \mu \mathbf{H} \cdot d\mathbf{a} \tag{18}$$

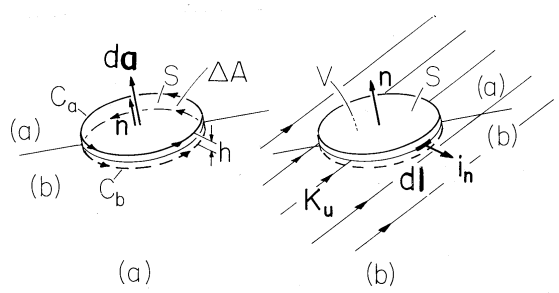


**Fig. 12.1.1** (a) Surface $S$ just above or just below the interface. (b) Volume $V$ of incremental thickness $h$ enclosing a section of the interface.

Whether taken on side (a) or side (b) of the interface, the line integral on the left is the same. This follows from Faraday's continuity law (16). Thus, if we take the difference between (18) evaluated on side (a) and on side (b), we obtain

$$\frac{d}{dt}(\mu_a \mathbf{H}^a - \mu_b \mathbf{H}^b) \cdot \mathbf{n} = 0 \tag{19}$$

By making the tangential electric field continuous, we have assured the continuity of the time derivative of the normal magnetic flux density. *For a sinusoidally time-dependent process, matching the tangential electric field automatically assures the matching of the normal magnetic flux densities.*

In particular, consider a surface of a conductor that is "perfect" in the MQS sense. The electric field inside such a conductor is zero. From (16), the tangential component of **E** just outside the conductor must also be zero. In view of (19), we conclude that the normal flux density at a perfectly conducting surface must be time independent. This boundary condition is familiar from the last half of Chap. 8.[2]

Given that the divergence of Ampère's law combines with Gauss' law to give conservation of charge,

$$\nabla \cdot \mathbf{J}_u + \frac{\partial \rho_u}{\partial t} = 0 \tag{20}$$

we should expect that there is a second relationship among the conditions of (14)–(17), this time between the surface charge density and surface current density that appear in the first two. Integration of (20) over the volume of the "pillbox" shown in Fig. 12.1.1b gives

$$\lim_{\substack{h \to 0 \\ \Delta A \to 0}} \left[ \oint_S \mathbf{J}_u \cdot d\mathbf{a} + \frac{d}{dt} \int_V \rho_u dV \right] = 0 \tag{21}$$

In the limit where first the thickness $h$ and then the area $\Delta A$ go to zero, these integrals reduce to $\Delta A$ times

$$\mathbf{n} \cdot (\mathbf{J}_u^a - \mathbf{J}_u^b) + \nabla_\Sigma \cdot \mathbf{K}_u + \frac{\partial \sigma_u}{\partial t} = 0 \tag{22}$$

[2] Note that the absence of a time-varying normal flux density does not imply that there is no tangential **E**. The surface of a material that is an infinite conductor in one direction but an insulator in the other might have no normal $\mu\mathbf{H}$ and yet support a tangential **E** in the direction of zero conductivity.

The first term is the contribution to the first integral in (21) from the surfaces on the (a) and (b) sides of the interface, respectively, having normals $+\mathbf{n}$ and $-\mathbf{n}$. The second term, which is written in terms of the "surface divergence" defined in terms of a vector $\mathbf{F}$ by

$$\nabla_\Sigma \cdot \mathbf{F} \equiv \lim_{\Delta A \to 0} \oint_C \mathbf{F} \cdot \mathbf{i}_n dl \tag{23}$$

results because the surface current density makes a finite contribution to the first integral in (21) even though the thickness $h$ of the volume goes to zero. [In (23), $\mathbf{i}_n$ is the unit normal to the volume $V$, as shown in the figure.] Such a surface current density can be used to represent currents imposed over a region having a thickness that is small compared to other dimensions of interest. It can also represent the current on the surface of a perfect conductor. (In using the conservation of charge continuity condition in Secs. 7.6 and 7.7, this term was not present because the surfaces described by this continuity condition were not carrying surface currents.) In terms of coordinates local to the point of interest, the surface divergence can be thought of as a two-dimensional divergence. The last term in (22) results from the integration of the charge density over the volume. Because there is a surface charge density, there is net charge inside the volume even in the limit where $h \to 0$.

When we specify $\mathbf{K}_u$ and $\sigma_u$ in (14) and (15), it is with the understanding that they obey the charge conservation continuity condition, (22). But, we also conclude that the charge conservation law is implied by the laws of Ampère and Gauss, and so we know that if (14) and (15) are satisfied, then so too is (22).

When perfectly conducting boundaries are described in Chaps. 13 and 14, the surface current and charge found on a perfectly conducting boundary using the continuity conditions from the laws of Ampère and Gauss will automatically satisfy the charge conservation condition. Further, a zero tangential electric field on a perfect conductor automatically implies that the normal magnetic flux density vanishes.

With the inhomogeneous wave equation playing the role of Poisson's equation, the stage is now set for a scenario paralleling that for electroquasistatics in Chap. 4 and for magnetoquasistatics in Chap. 8. The next section identifies the fields associated with source singularities. Section 12.3 develops superposition integrals for the response to given distributions of the sources. Henceforth, in this and the next chapter, we shall drop the subscript $u$ from the source quantities.

## 12.2 ELECTRODYNAMIC FIELDS OF SOURCE SINGULARITIES

Given the response to an elemental source, the fields associated with an arbitrary distribution of sources can be found by superposition. This approach will be formalized in the next section and can be utilized for determining the radiation patterns of many antenna arrays. The fields resulting from this superposition principle form a particular solution that can be combined with solutions to the homogeneous wave equation to satisfy the boundary conditions imposed by perfectly conducting boundaries.

We begin by identifying the potential $\Phi$ associated with a time varying point charge $q(t)$. In a closed system, where the net charge is invariant, an increase in

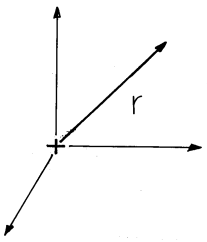


**Fig. 12.2.1** A point charge located at the origin of a spherical coordinate system.

charge at one point must be compensated by a decrease in charge elsewhere. Thus, as we shall see in identifying the fields of an electric dipole, physically meaningful fields are the superposition of those produced by at least two point charges of opposite sign. Conservation of charge further requires that this shift in the distribution of net charge from one region to another be accounted for by a current. This current is the source term in the inhomogeneous wave equation for the vector potential.

**Potential of a Point Charge.** Consider the potential $\Phi$ predicted by the inhomogeneous wave equation, (12.1.10), for a time varying point charge $q(t)$ located at the origin of the spherical coordinate system shown in Fig. 12.2.1.

By definition, $\rho$ is zero everywhere except at the origin, where it is singular.[3] In the immediate neighborhood of the origin, we should expect that the potential varies so rapidly with $r$ that the Laplacian would dominate the second time derivative in the inhomogeneous wave equation, (12.1.10). Then, in the vicinity of the origin, we should expect the potential for a point charge to be the same as for Poisson's equation, namely $q(t)/(4\pi\epsilon r)$ (4.4.1). From Sec. 3.1, we have a hint as to how the combined effects of the magnetic induction and electric displacement current represented by the second time derivative in the inhomogeneous wave-equation, (12.1.10), should affect this potential. We can expect that the response at a radial position $r$ will be delayed by the time required for an electromagnetic wave to reach that position from the origin. For a wave propagating at the velocity $c$, this time is $r/c$. Thus, we make the educated guess that the solution to (12.1.10) for a point charge at the origin is

$$\Phi = \frac{q\left(t - \frac{r}{c}\right)}{4\pi\epsilon r} \tag{1}$$

where $c = 1/\sqrt{\mu\epsilon}$. According to (1), given that the time dependence of the point charge is $q(t)$, the potential at radius $r$ is given by the familiar potential for a point charge, provided that $t \to (t - r/c)$.

Verification that $\Phi$ of (1) is a solution to the inhomogeneous wave equation (12.1.10) takes two steps. First, the expression is substituted into the *homogeneous* wave equation [(12.1.10) with no source] to see that it is satisfied everywhere except at the origin. In carrying out this step, note that $\Phi$ is a function of the spherical

[3] Of course, charge conservation requires that there be a current supplying this time-varying charge and that through action of this current, if charge accumulates at the origin, there must be a reduction of charge somewhere else. The simplest example of a source obeying charge conservation is the dipole.

radial coordinate $r$ alone. Thus, $\nabla^2\Phi$ is simply $r^{-2}\partial(r^2\partial\Phi/\partial r)/\partial r$. This operation gives the same result as the operation $r^{-1}\partial^2(r\Phi)/\partial r^2$. Thus, evaluated using the potential of (1), the terms on the left in the inhomogeneous wave equation, (12.1.10), become

$$\nabla^2\Phi - \frac{1}{c^2}\frac{\partial^2\Phi}{\partial t^2} = \frac{1}{4\pi\epsilon}\left[\frac{1}{r}\frac{\partial^2}{\partial r^2}q\big(t-\frac{r}{c}\big) - \frac{1}{r}\frac{1}{c^2}\frac{\partial^2}{\partial t^2}q\big(t-\frac{r}{c}\big)\right] = 0 \tag{2}$$

for $r \neq 0$. In carrying out this evaluation, note that $\partial q/\partial r = -q'/c$ and $\partial q/\partial t = q'$ where the prime indicates a derivative with respect to the argument. Thus, the homogeneous wave equation is satisfied everywhere except at the origin.

In the second step, we confirm that (1) is the dynamic potential of a point charge. We integrate the inhomogeneous wave equation in the neighborhood of $r = 0$, (12.1.10), over a small spherical volume of radius $r$ centered on the origin.

$$\int_V \Big( -\nabla\cdot\nabla\Phi + \mu\epsilon\frac{\partial^2\Phi}{\partial t^2}\Big)dv = \int_V \frac{\rho}{\epsilon}dv \tag{3}$$

The Laplacian has been written in terms of its definition in anticipation of using Gauss' theorem to convert the first integral to one over the surface at $r$. In the limit where $r$ is small, the integration of the second time derivative term gives no contribution.

$$\begin{aligned}\int_V \mu\epsilon\frac{\partial^2\Phi}{\partial t^2}dv &= \mu\epsilon\frac{\partial^2}{\partial t^2}\lim_{r\to 0}\int_V \Phi dv \\ &= \mu\epsilon\frac{\partial^2}{\partial t^2}\lim_{r\to 0}\int_0^r \frac{q4\pi r^2}{4\pi\epsilon r}dr = 0\end{aligned} \tag{4}$$

Integration of the first term on the left in (3) is familiar from Chap. 4, because Gauss' theorem converts the volume integration to one over the enclosing surface and we therefore have

$$\begin{aligned}-\int \nabla\cdot\nabla\Phi dv &= -\oint_S \nabla\Phi\cdot d\mathbf{a} = -4\pi r^2\frac{\partial\Phi}{\partial r} \\ &= -4\pi r^2\big(-\frac{q}{4\pi\epsilon r^2}\big) = \frac{q}{\epsilon}\end{aligned} \tag{5}$$

In the limit where $r \to 0$, the integral on the right in (3) gives $q/\epsilon$. Thus, it reduces to the same expression obtained using (1) to evaluate the left-hand side of (3). We conclude that (1) is indeed the solution to the inhomogeneous wave equation for a point charge at the origin.

**Electric Dipole Field.** An electric dipole consists of a pair of charges $\pm q(t)$ separated by the distance $d$, as shown in Fig. 12.2.2. As one charge increases in magnitude at the expense of the other, there is an elemental current $i(t)$ directed between the two along the $z$ axis. Charge conservation requires that

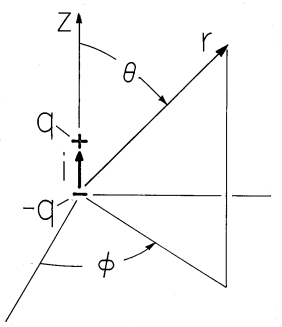


**Fig. 12.2.2** A dynamic dipole in which the time-variation of the charge is accounted for by the elemental current $i(t)$.

$$\boxed{i = \frac{dq}{dt}} \tag{6}$$

This current can be pictured as a singularity in the distribution of the current density $J_z$. In fact, the role played by $\rho/\epsilon$ as the source of $\Phi$ on the right in (12.1.10) is played by $\mu J_z$ in determining $A_z$ in (12.1.8). Just as $q$ can be regarded as the integral of the charge density $\rho$ over the elemental volume occupied by that charge density, $\mu id$ is $\mu J_z$ first integrated over the cross-sectional area in the $x-y$ plane of the current tube joining the charges (to give $\mu i$) and then integrated over the length $d$ of the tube. Thus, we exploit the analogy between the $z$ component of the vector inhomogeneous wave equation for $A_z$ and that for $\Phi$, (12.1.8) and (12.1.10), to write the vector potential associated with an incremental current element at the origin. The solution to (12.1.8) is the same as that to (12.1.10) with $q/\epsilon \to \mu id$.

$$\boxed{A_z = \frac{\mu d i\left(t - \frac{r}{c}\right)}{4\pi r}} \tag{7}$$

Remember that $r$ is a spherical coordinate, so it is best to convert this expression into spherical coordinates. Figure 12.2.3 shows that

$$A_r = A_z \cos\theta; \qquad A_\theta = -A_z \sin\theta \tag{8}$$

Thus, in spherical coordinates, (7) becomes the vector potential for an electric dipole.

$$\mathbf{A} = \frac{\mu d}{4\pi}\left[\frac{i\left(t - \frac{r}{c}\right)}{r}\cos\theta \mathbf{i}_\mathbf{r} - \frac{i\left(t - \frac{r}{c}\right)}{r}\sin\theta \mathbf{i}_\theta\right] \tag{9}$$

The dipole scalar potential is the superposition of the potentials due to the individual charges, (5). The positive charge is located on the $z$ axis at $z = d$, while the negative one is at the origin, so superposition gives

$$\Phi = \frac{1}{4\pi\epsilon}\left\{\frac{q\left[t - \left(\frac{r}{c} - \frac{d}{c}\cos\theta\right)\right]}{r - d\cos\theta} - \frac{q\left[t - \frac{r}{c}\right]}{r}\right\} \tag{10}$$

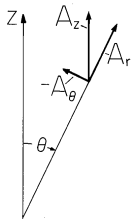


**Fig. 12.2.3** The $z$-directed potential is analyzed into its components in spherical coordinates.

where, in a way familiar from Sec. 4.4, the distance from the point of observation to the charge at $z = d$ is approximated by $r - d\cos\theta$. With $q'$ indicating a derivative with respect to the argument, expansion in a Taylor's series based on $d\cos\theta \ll r$ gives

$$\Phi \simeq \frac{1}{4\pi\epsilon}\left\{\left(\frac{1}{r}+\frac{d\cos\theta}{r^2}\right)q\big(t-\frac{r}{c}\big)+\frac{d}{c}\frac{\cos\theta}{r}q'\big(t-\frac{r}{c}\big)-\frac{q\big(t-\frac{r}{c}\big)}{r}\right\} \tag{11}$$

and keeping terms that are linear in $d$ results in the desired scalar potential for the electric dipole.

$$\Phi = \frac{d}{4\pi\epsilon}\left[\frac{q\big(t-\frac{r}{c}\big)}{r^2}+\frac{q'\big(t-\frac{r}{c}\big)}{cr}\right]\cos\theta \tag{12}$$

The vector potential (9) and scalar potential (12) obey (12.1.7), as can be confirmed by differentiation and use of the conservation law (6). We can now evaluate the magnetic and electric fields associated with these scalar and vector potentials. The magnetic field intensity follows by evaluating (12.1.1) using (9). [Remember that conservation of charge requires that $q' = i$, in accordance with (6).]

$$\boxed{\mathbf{H} = \frac{d}{4\pi}\left[\frac{i'\big(t-\frac{r}{c}\big)}{cr}+\frac{i\big(t-\frac{r}{c}\big)}{r^2}\right]\sin\theta\mathbf{i}_\phi} \tag{13}$$

To find $\mathbf{E}$, (12.1.3) is evaluated using (9) and (12).

$$\boxed{\begin{aligned}\mathbf{E} = \frac{d}{4\pi\epsilon}\Bigg\{&2\left[\frac{q\big(t-\frac{r}{c}\big)}{r^3}+\frac{q'\big(t-\frac{r}{c}\big)}{cr^2}\right]\cos\theta\mathbf{i}_\mathbf{r}\\&+\left[\frac{q\big(t-\frac{r}{c}\big)}{r^3}+\frac{q'\big(t-\frac{r}{c}\big)}{cr^2}+\frac{q''\big(t-\frac{r}{c}\big)}{c^2r}\right]\sin\theta\mathbf{i}_\theta\Bigg\}\end{aligned}} \tag{14}$$

As can be seen by comparing (14) to (4.4.10), in the limit where $c \to \infty$, this electric field becomes the electric field found from the electroquasistatic dipole potential. Note that the quasistatic field is proportional to $q$ (rather than its first or second temporal derivative) and decays as $1/r^3$. The first and second time derivatives of $q$ are of order $q/\tau$ and $q/\tau^2$ respectively, where $\tau$ is the typical time interval

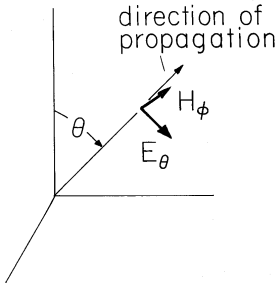


**Fig. 12.2.4** Far fields constituting a plane wave propagating in the radial direction.

within which $q$ experiences an appreciable change. Thus, these time derivative terms are small compared to the quasistatic terms if $r/c \ll \tau$. What we have found gives substance to the arguments given for the EQS approximation in Sec. 3.3. That is, we have found that the quasistatic approximation is justified if the condition of (3.3.5) prevails.

The combination of electric displacement current and magnetic induction leading to the inhomogeneous wave equation has three dramatic effects on the dipole fields. First, the response at a location $r$ is delayed[4] by the transit time $r/c$. Second, the electric field is not only proportional to $q(t-r/c)$, but also to $q'(t-r/c)$ and $q''(t-r/c)$. Third, the part of the electric field that is proportional to $q''$ decreases with radius in proportion to $1/r$. Associated with this "far field" is a magnetic field, the first term in (13), that similarly decreases as $1/r$. Together, these fields comprise an electromagnetic wave propagating radially outward from the dipole antenna.

$$\begin{aligned} \lim_{r\to\infty} \mathbf{H} &\to \frac{d}{4\pi}\frac{i'\left(t-\frac{r}{c}\right)\sin\theta \mathbf{i}_\phi}{cr} \\ \lim_{r\to\infty} \mathbf{E} &\to \frac{d}{4\pi\epsilon}\frac{q''\left(t-\frac{r}{c}\right)}{c^2 r}\sin\theta \mathbf{i}_\theta \end{aligned} \tag{15}$$

Note that these field components are orthogonal to each other and transverse to the radial direction of propagation, as shown in Fig. 12.2.4.

To appreciate the significance of the $1/r$ dependence of the fields in (15), consider the Poynting flux, (11.2.9), associated with these fields.

$$\lim_{r\to\infty}[\mathbf{E}\times\mathbf{H}] = \left(\frac{d}{4\pi}\right)^2\sqrt{\mu/\epsilon}\frac{\left[q''\left(t-\frac{r}{c}\right)\right]^2}{c^2 r^2}\sin^2\theta \tag{16}$$

The power flow out through a spherical surface at the radius $r$ follows from this expression as

$$\begin{aligned} P = \oint \mathbf{E}\times\mathbf{H}\cdot d\mathbf{a} &= \int_0^\pi \left(\frac{d}{4\pi}\right)^2\sqrt{\mu/\epsilon}\frac{(q'')^2}{c^2 r^2}\sin^2\theta 2\pi r^2\sin\theta d\theta \\ &= \frac{d^2}{6\pi}\sqrt{\mu/\epsilon}\frac{\left[q''\left(t-\frac{r}{c}\right)\right]^2}{c^2} \end{aligned} \tag{17}$$

[4] In addition to the retarded response highlighted here, an "advanced" response, where $t-r/c \to t+r/c$, is also a solution to the inhomogeneous wave equation. Because it does not fit with our idea of causality, it is not used here.

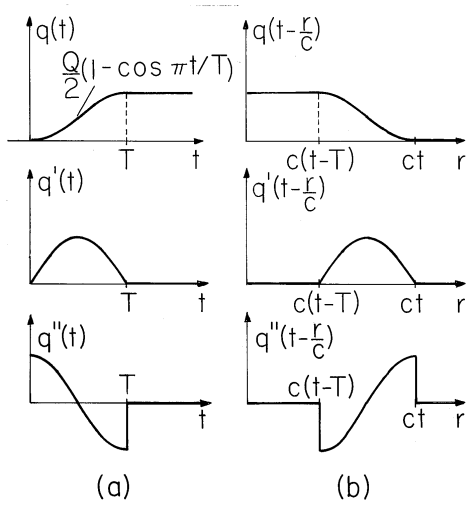


**Fig. 12.2.5** (a) Time dependence of the dipole charge $q(t)$ as well as its first and second derivatives. (b) The radial dependence of the functions needed to evaluate the dipole fields resulting from the turn-on transient of (a) when $t > T$.

Because the far fields of the dipole vary as $1/r$, and hence the power flux density is proportional to $1/r^2$, and because the area of the surface at $r$ increases as $r^2$, we conclude that there is a net power flowing outward from the dipole at infinity. These far field components are called the *radiation field.*

**Example 12.2.1.** Turn-on Fields of an Electric Dipole

To help establish the physical significance of the electric dipole expressions for **E** and **H**, (13) and (14), consider the fields associated with charging an electric dipole through the transient shown in Fig. 12.2.5a. Over a period $T$, the charge increases from zero to $Q$ with a continuous first derivative but a second derivative that suffers a finite discontinuity, as shown in the figure. Multiplied by appropriate factors of $1/r$, $1/r^2$, and $1/r^3$, the field distributions are made up of these three functions, with $t$ replaced by $t - r/c$. Thus, at a given instant in time, the factors $q(t - r/c)$, $q'(t - r/c)$, and $q''(t - r/c)$ have the radial distributions shown in Fig. 12.2.5b.

The electric and magnetic fields are shown at three successive instants in time in Fig. 12.2.6. The transient part of the field is confined to an annular region with its outside radius at $r = ct$ (the wave front) and inner radius at $r = c(t - T)$. Inside this latter radius, the fields are static and composed only of those terms varying as $1/r^3$. Thus, when $t = T$ (Fig. 12.2.6a), all of the field is transient, because the source has just reached a constant state. At the subsequent times $t = 2T$ and $t = 3T$, the fields left behind by the outward propagating rear of the wave transient, the **E** field of a static electric dipole and $\mathbf{H} = \mathbf{0}$, are as shown in Figs. 12.2.6b and 6c.

The flow of charges to the poles of the dipole produces an electromagnetic wave which reveals its identity once the annular region of the transient fields propagates out of the range of the near field. Note that the electric and magnetic fields shown in the outward propagating wave of Fig. 12.2.6c are mutually sustaining. In accordance with Faradays' law, the curl of **E**, which is $\phi$ directed and tends to be largest midway

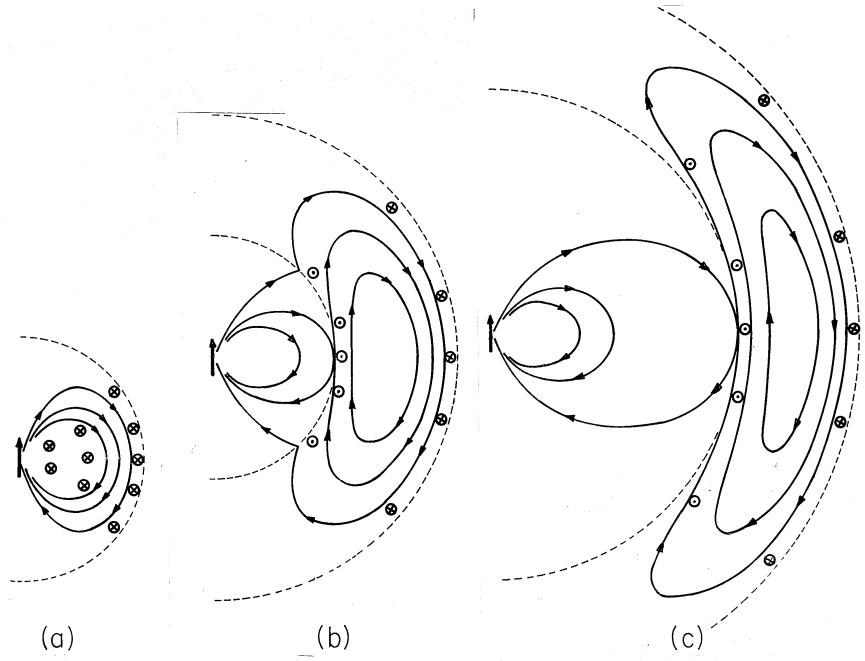


**Fig. 12.2.6** Electric fields (solid lines) and magnetic fields resulting from turning on an electric dipole in accordance with the temporal dependence indicated in Fig. 12.2.5. The fields are zero outside the wave front indicated by the outermost broken line. (a) For $t < T$, the entire field is in a transient state. (b) By the time $t > T$, the fields due to the transient are seen to be propagating outward between the expanding spherical surfaces at $r = ct$ and $r = c(t - T)$. Inside the latter surface, which is also indicated by a broken line, the fields are static. (c) At still later times, the propagating wave divorces itself from the dipole as the electric field generated by the magnetic induction, and the magnetic field generated by the displacement current, become self-sustaining.

between the front and back of the wave, is balanced by a time rate of change of $\mathbf{B}$ which also has its largest value in the same region.[5] Similarly, to satisfy Ampère's law, the $\theta$-directed curl of $\mathbf{H}$, which also peaks midway between the front and back of the wave, is balanced by a time rate of change of $\mathbf{D}$ that peaks in the same region.

It is instructive to review the discussion given in Sec. 3.3 of EQS and MQS approximations and their relation to electromagnetic waves. The electric dipole considered here in detail is the prototype system sketched in Fig. 3.3.1a. We have indeed found that if the condition of (3.3.5) is met, the EQS fields dominate. We should expect that if the current carried by the elemental loop of the prototype MQS system of Fig. 3.3.1b is a rapidly varying function of time, then the magnetic dipole (considered in the MQS limit in Sec. 8.3) also gives rise to a radiation field

[5] In discerning a time rate of change implied by the figure, remember that the fields in the region of the spherical shell indicated by the two broken-line circles in Figs. 12.2.6b and 12.2.6c are propagating outward.

much like that discussed here. These fields are considered at the conclusion of this section.

**Electric Dipole in the Sinusoidal Steady State.** In the sections that follow, the fields of the electric dipole will be superimposed to obtain field patterns from antennae used at radio and microwave frequencies. In most of these practical situations, the field sources, $q$ and $i$, are essentially in the sinusoidal steady state. In particular,

$$i = \text{Re } \hat{i}e^{j\omega t} \tag{18}$$

where $\hat{i}$ is a complex number representing both the phase and amplitude of the current. Then, the general expression for the vector potential of the electric dipole, (7), becomes

$$A_z = \text{Re } \frac{\mu d\hat{i}}{4\pi r} e^{j\omega(t-\frac{r}{c})} \tag{19}$$

Separation of the time dependence from the space dependence in solving the inhomogeneous wave equation is accomplished by the use of complex vector functions of space multiplied by $\exp j\omega t$. With the understanding that the time dependence is recovered by multiplying by $\exp(j\omega t)$ and taking the real part, we will now deal with the complex amplitudes of the fields and drop the factor $\exp j\omega t$. Thus, (19) becomes

$$A_z = \text{Re } \hat{A}_z e^{j\omega t}; \qquad \hat{A}_z = \frac{\mu d\hat{i}}{4\pi} \frac{e^{-jkr}}{r} \tag{20}$$

where the *wave number* $k \equiv \omega/c$.

In terms of complex amplitudes, the magnetic and electric field intensities of the electric dipole follow from (13) and (14) as [by substituting $q \rightarrow \text{Re } (\hat{i}/j\omega) \exp(-jkr) \exp(j\omega t)$]

$$\hat{\mathbf{H}} = j\frac{kd\hat{i}}{4\pi}\left(\frac{1}{jkr} + 1\right) \sin\theta \frac{e^{-jkr}}{r} \mathbf{i}_\phi \tag{21}$$

$$\begin{aligned} \hat{\mathbf{E}} = & j\frac{kd\hat{i}}{4\pi}\sqrt{\mu/\epsilon}\left\{2\left[\frac{1}{(jkr)^2} + \frac{1}{jkr}\right]\cos\theta \mathbf{i}_\mathbf{r}\right. \\ & \left. + \left[\frac{1}{(jkr)^2} + \frac{1}{jkr} + 1\right]\sin\theta \mathbf{i}_\theta\right\}\frac{e^{-jkr}}{r} \end{aligned} \tag{22}$$

The far fields are given by terms with the $1/r$ dependence.

$$\boxed{\hat{H}_\phi = j\frac{kd\hat{i}}{4\pi}\sin\theta\frac{e^{-jkr}}{r}} \tag{23}$$

$$\boxed{\hat{E}_\theta = \sqrt{\mu/\epsilon}\hat{H}_\phi} \tag{24}$$

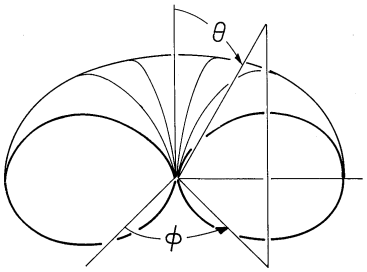


**Fig. 12.2.7** Radiation pattern of short electric dipole, shown in the range $\pi/2 < \phi < 3\pi/2$.

These fields, which are a special case of those pictured in Fig. 12.2.4, propagate radially outward. The far field pattern is a radial progression of the fields shown between the broken lines in Fig. 12.2.6c. (The response shown is the result of one half of a cycle.)

It follows from (23) and (24) that for a short dipole in the sinusoidal steady state, the power radiated per unit solid angle is[6]

$$\frac{4\pi r^2\langle S_r\rangle}{4\pi} = r^2\frac{1}{2}\mathrm{Re}\,\hat{\mathbf{E}}\times\hat{\mathbf{H}}^*\cdot\mathbf{i_r} = \frac{1}{2}\sqrt{\mu/\epsilon}\frac{(kd)^2}{(4\pi)^2}|\hat{i}|^2\sin^2\theta \tag{25}$$

Equation (25) expresses the dependence of the radiated power on the direction $(\theta,\phi)$, and can be called the radiation pattern. Often, only the functional dependence, $\Psi(\theta,\phi)$ is identified with the "radiation pattern." In the case of the short electric dipole,

$$\Psi(\theta,\phi) = \sin^2\theta \tag{26}$$

and the radiation pattern is as shown in Fig. 12.2.7.

**The Far-Field and Uniformly Polarized Plane Waves.** For an observer far from the dipole, the variation of the field with respect to radius is more noticeable than that with respect to the angle $\theta$. Further, if $kr$ is large, the radial variation represented by $\exp(-jkr)$ dominates over the much weaker dependence due to the factor $1/r$. This term makes the fields tend to repeat themselves every wavelength $\lambda = 2\pi/k$. At frequencies of the order used for VHF television, the wavelength is on the order of a meter, while the station antenna is typically kilometers away. Thus, over the dimensions of a receiving antenna, the variations due to the factor $1/r$ and the $\theta$ variation in (23) and (24) are insignificant. By contrast, the receiving antenna has dimensions on the order of $\lambda$, and so the radial variation represented by $\exp(-jkr)$ is all-important. Far from the dipole, where spatial variations transverse to the radial direction of propagation are unimportant, and where the slow decay due to the $1/r$ term is negligible, the fields take the form of *uniform plane waves*. With the local spherical coordinates replaced by Cartesian coordinates, as shown in Fig. 12.2.8, the fields then take the form

$$\mathbf{E} = E_z(y,t)\mathbf{i_z}; \qquad \mathbf{H} = H_x(y,t)\mathbf{i_x} \tag{27}$$

[6] Here we use the time average theorem of (11.5.6).

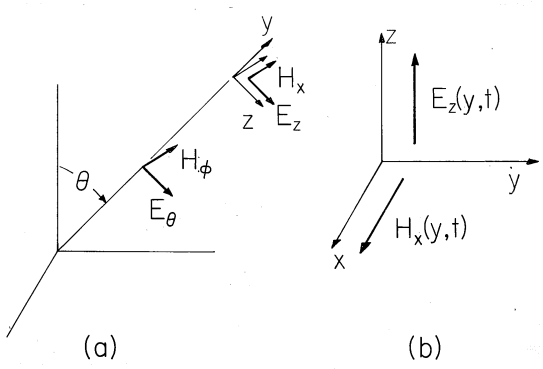


**Fig. 12.2.8** (a) Radiation field of electric dipole. (b) Cartesian representation in neighborhood of remote point.

That is, the fields depend only on $y$, which plays the role of $r$, and are directed transverse to $y$. Instead of the far fields given by (15), we have traveling-wave fields that, by virtue of their independence of the transverse coordinates, are called *plane waves*. To emphasize that the dipole has indeed launched a plane wave, in (15) we replace

$$\frac{d}{4\pi\epsilon}\frac{q''(t-\frac{r}{c})}{c^2 r}\sin\theta \rightarrow E_+(t-\frac{y}{c}) \tag{28}$$

and recognize that $i' = q''$, (6), so that

$$\mathbf{E} = E_+(t-\frac{y}{c})\mathbf{i_z}; \qquad \mathbf{H} = \sqrt{\epsilon/\mu}E_+(t-\frac{y}{c})\mathbf{i_x} \tag{29}$$

The dynamics of such plane waves are described in Chap. 14. Note that the ratio of the magnitudes of $\mathbf{E}$ and $\mathbf{H}$ is the *intrinsic impedance* $\zeta \equiv \sqrt{\mu/\epsilon}$. In free space, $\zeta = \zeta_o \equiv \sqrt{\mu_o/\epsilon_o} \approx 377\Omega$.

**Magnetic Dipole Field.** Given the magnetic and electric fields of an electric dipole, (13) and (14), what are the electrodynamic fields of a magnetic dipole? We answer this question by exploiting a far-reaching property of Maxwell's equations, (12.0.7)–(12.0.10), as they apply where $\mathbf{J}_u = 0$ and $\rho_u = 0$. In such regions, Maxwell's equations are replicated by replacing $\mathbf{H}$ by $-\mathbf{E}$, $\mathbf{E}$ by $\mathbf{H}$, $\epsilon$ by $\mu$, and $\mu$ by $\epsilon$. It follows that because (13) and (14) are solutions to Maxwell's equations, then so are the fields.

$$\mathbf{E} = -\frac{d}{4\pi}(\frac{q''_m}{cr} + \frac{q'_m}{r^2})\sin\theta\mathbf{i}_\phi \tag{30}$$

$$\mathbf{H} = \frac{d}{4\pi\mu}\left[2(\frac{q_m}{r^3} + \frac{q'_m}{cr^2})\cos\theta\mathbf{i_r} + (\frac{q_m}{r^3} + \frac{q'_m}{cr^2} + \frac{q''_m}{c^2 r})\sin\theta\mathbf{i}_\theta\right] \tag{31}$$

Of course, $q_m$ must now be interpreted as a source of divergence of $\mathbf{H}$, i.e., a magnetic charge. Substitution shows that these fields do indeed satisfy Maxwell's equations with $\mathbf{J} = 0$ and $\rho = 0$, except at the origin. To discover the source singularity at the origin giving rise to these fields, they are examined in the limit

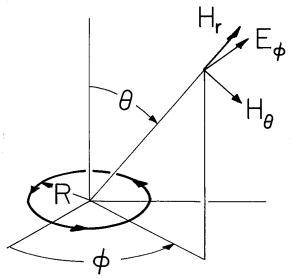


**Fig. 12.2.9** Magnetic dipole giving rise to the fields of (33) and (34).

where $r \to 0$. Observe that in the neighborhood of the origin, terms proportional to $1/r^3$ dominate $\mathbf{H}$ as given by (31). Close to the source, $\mathbf{H}$ takes the form of a magnetic dipole. This can be seen by a comparison of this near field to that given by (8.3.20) for a magnetic dipole.

$$dq_m\big(t-\frac{r}{c}\big)=\mu m\big(t-\frac{r}{c}\big) \tag{32}$$

With this identification of the source, (30) and (31) become

$$\boxed{\mathbf{E}=-\frac{\mu}{4\pi}\left[\frac{m''\big(t-\frac{r}{c}\big)}{cr}+\frac{m'\big(t-\frac{r}{c}\big)}{r^2}\right]\sin\theta\mathbf{i}_\phi} \tag{33}$$

$$\boxed{\begin{aligned}\mathbf{H}=\frac{1}{4\pi}\Bigg\{&2\left[\frac{m\big(t-\frac{r}{c}\big)}{r^3}+\frac{m'\big(t-\frac{r}{c}\big)}{cr^2}\right]\cos\theta\mathbf{i}_\mathbf{r}\\&+\left[\frac{m\big(t-\frac{r}{c}\big)}{r^3}+\frac{m'\big(t-\frac{r}{c}\big)}{cr^2}+\frac{m''\big(t-\frac{r}{c}\big)}{c^2r}\right]\sin\theta\mathbf{i}_\theta\Bigg\}\end{aligned}} \tag{34}$$

The small current loop of Fig. 12.2.9, which has a magnetic moment $m=\pi R^2 i$, could be the source of the fields given by (33) and (34). If the current driving this loop were turned on in a manner analogous to that considered in Example 12.2.1, the field left behind the outward propagating pulse would be the magnetic dipole field derived in Example 8.3.2.

The complex amplitudes of the far fields for the magnetic dipole are the counterpart of the fields given by (23) and (24) for an electric dipole. They follow from the first term of (33) and the last term of (34) as

$$\boxed{\hat{H}_\theta=-\frac{k^2}{4\pi}\hat{m}\sin\theta\frac{e^{-jkr}}{r}} \tag{35}$$

$$\boxed{\hat{E}_\phi=-\sqrt{\mu/\epsilon}\hat{H}_\theta} \tag{36}$$

In Sec. 12.4, it will be seen that the radiation fields of the electric dipole can be superimposed to describe the radiation patterns of current distributions and of antenna arrays. A similar application of (35) and (36) to describing the radiation patterns of antennae composed of arrays of magnetic dipoles is illustrated by the problems.

## 12.3 SUPERPOSITION INTEGRAL FOR ELECTRODYNAMIC FIELDS

With the identification in Sec. 12.2 of the fields associated with point charge and current sources, we are ready to construct fields produced by an arbitrary distribution of sources. Just as the superposition integral of Sec. 4.5 was based on the linearity of Poisson's equation, the superposition principle for the dynamic fields hinges on the linear nature of the inhomogeneous wave equations of Sec. 12.1.

**Transient Response.** The scalar potential for a point charge $q$ at the origin, given by (12.2.1), can be generalized to describe a point charge at an arbitrary source position $\mathbf{r}'$ by replacing the distance $r$ by $|\mathbf{r}-\mathbf{r}'|$ (see Fig. 4.5.1). Then, the point charge is replaced by the charge density $\rho$ evaluated at the source position multiplied by the incremental volume element $dv'$. With these substitutions in the scalar potential of a point charge, (12.2.1), the potential at an observer location $\mathbf{r}$ is the integrand of the expression

$$\boxed{\Phi(\mathbf{r},t)=\int_{V'}\frac{\rho\left(\mathbf{r}',\ t-\frac{|\mathbf{r}-\mathbf{r}'|}{c}\right)}{4\pi\epsilon|\mathbf{r}-\mathbf{r}'|}dv'} \tag{1}$$

The integration over the source coordinates $\mathbf{r}'$ then superimposes the fields at $\mathbf{r}$ due to all of the sources. Given the charge density everywhere, this integral comprises the solution to the inhomogeneous wave equation for the scalar potential, (12.1.10).

In Cartesian coordinates, any one of the components of the vector inhomogeneous wave-equation, (12.1.8), obeys a scalar equation. Thus, with $\rho/\epsilon \rightarrow \mu J_i$, (1) becomes the solution for $A_i$, whether $i$ be $x$, $y$ or $z$.

$$\boxed{\mathbf{A}(\mathbf{r},t)=\mu\int_{V'}\frac{\mathbf{J}\left(\mathbf{r}',\ t-\frac{|\mathbf{r}-\mathbf{r}'|}{c}\right)}{4\pi|\mathbf{r}-\mathbf{r}'|}dv'} \tag{2}$$

We should keep in mind that conservation of charge implies a relationship between the current and charge densities of (1) and (2). Given the current density, the charge density is determined to within a time-independent distribution. An alternative, and often less involved, approach to finding $\mathbf{E}$ avoids the computation of the charge density. Given $\mathbf{J}$, $\mathbf{A}$ is found from (2). Then, the gauge condition, (12.1.7), is used to find $\Phi$. Finally, $\mathbf{E}$ is found from (12.1.3).

**Sinusoidal Steady State Response.** In many practical situations involving radio, microwave, and optical frequency systems, the sources are essentially in the sinusoidal steady state.

$$\rho = \text{Re}\ \hat{\rho}(\mathbf{r})e^{j\omega t} \Rightarrow \Phi = \text{Re}\hat{\Phi}(\mathbf{r})e^{j\omega t} \tag{3}$$

Equation (1) is evaluated by using the charge density given by (3), with $\mathbf{r} \rightarrow \mathbf{r}'$ and $t \rightarrow t - |\mathbf{r} - \mathbf{r}'|/c$

$$\begin{aligned} \Phi &= \text{Re} \int_{V'} \frac{\hat{\rho}(\mathbf{r}')e^{j\omega\left(t - \frac{|\mathbf{r}-\mathbf{r}'|}{c}\right)}}{4\pi\epsilon|\mathbf{r} - \mathbf{r}'|} dv' \\ &= \text{Re}\left[\int_{V'} \frac{\hat{\rho}(\mathbf{r}')e^{-jk|\mathbf{r}-\mathbf{r}'|}}{4\pi\epsilon|\mathbf{r} - \mathbf{r}'|} dv'\right] e^{j\omega t} \end{aligned} \tag{4}$$

where $k \equiv \omega/c$. Thus, the quantity in brackets in the second expression is the complex amplitude of $\Phi$ at the location $\mathbf{r}$. With the understanding that the time dependence will be recovered by multiplying this complex amplitude by $\exp(j\omega t)$ and taking the real part, the superposition integral for the complex amplitude of the potential is

$$\boxed{\hat{\Phi} = \int_{V'} \frac{\hat{\rho}(\mathbf{r}')e^{-jk|\mathbf{r}-\mathbf{r}'|}}{4\pi\epsilon|\mathbf{r} - \mathbf{r}'|} dv'} \tag{5}$$

From (2), the same reasoning gives the superposition integral for the complex amplitude of the vector potential.

$$\boxed{\hat{\mathbf{A}} = \frac{\mu}{4\pi} \int_{V'} \frac{\hat{\mathbf{J}}(\mathbf{r}')e^{-jk|\mathbf{r}-\mathbf{r}'|}}{|\mathbf{r} - \mathbf{r}'|} dv'} \tag{6}$$

The superposition integrals are often used to find the radiation patterns of driven antenna arrays. In these cases, the distribution of current, and hence charge, is independently prescribed everywhere. Section 12.4 illustrates this application of the superposition integral.

If fields are to be found in confined regions of space, with part of the source distribution on boundaries, the fields given by the superposition integrals represent particular solutions to the inhomogeneous wave equations. Following the same approach as used in Sec. 5.1 for solving boundary value problems involving Poisson's equation, the boundary conditions can then be satisfied by superimposing on the solution to the *inhomogeneous* wave equation solutions satisfying the *homogeneous* wave equation.

## 12.4 ANTENNA RADIATION FIELDS IN THE SINUSOIDAL STEADY STATE

Antennae are designed to transmit and receive electromagnetic waves. As we know from Sec. 12.2, the superposition integrals for the scalar and vector potentials result

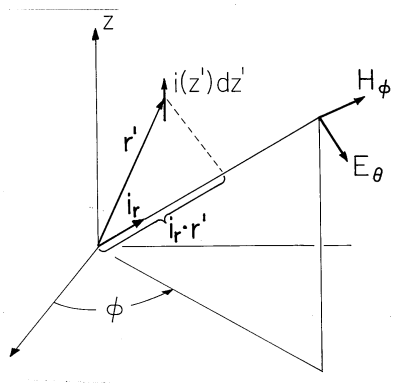


**Fig. 12.4.1** Incremental current element at $\mathbf{r}'$ is source for radiation field at $(r, \theta, \phi)$.

in both the radiation and near fields. If we confine our interest to the fields far from the antenna, extensive simplifications are achieved.

Many types of antennae are composed of driven conducting elements that are extremely thin. This often makes it possible to use simple arguments to approximate the distribution of current over the length of the conductor. With the current distribution specified at the outset, the superposition integrals of Sec. 12.3 can then be used to determine the associated fields.

An element $idz'$ of the current distribution of an antenna is pictured in Fig. 12.4.1 at the source location $\mathbf{r}'$. If this element were at the origin of the spherical coordinate system shown, the associated radiation fields would be as given by (12.2.23) and (12.2.24). With the distance to the current element $r'$ much less than $r$, how do we adapt these expressions so that they represent the fields when the incremental source is located at $\mathbf{r}'$ rather than at the origin?

The current elements comprising the antenna are typically within a few wavelengths of the origin. By contrast, the distance $r$ (say, from a TV transmitting antenna, where the wavelength is on the order of 1 meter, to a receiver 10 kilometers away) is far larger. For an observer in the neighborhood of a point $(r, \theta, \phi)$, there is little change in $\sin\theta/r$, and hence in the *magnitude* of the field, caused by a displacement of the current element from the origin to $\mathbf{r}'$. However, the *phase* of the electromagnetic wave launched by the current element is strongly influenced by changes in the distance from the element to the observer that are of the order of a wavelength. This is seen by writing the argument of the exponential term in terms of the wavelength $\lambda$, $jkr = j2\pi r/\lambda$.

With the help of Fig. 12.4.1, we see that the distance from the source to the observer is $r - \mathbf{r}' \cdot \mathbf{i}_\mathbf{r}$. Thus, for the current element located at $\mathbf{r}'$ in the neighborhood of the origin, the radiation fields given by (12.2.23) and (12.2.24) are

$$\boxed{\hat{H}_\phi \simeq \frac{jk}{4\pi} \sin\theta \frac{e^{-jk(r-\mathbf{r}'\cdot\mathbf{i}_\mathbf{r})}}{r} i(\mathbf{r}')dz'} \tag{1}$$

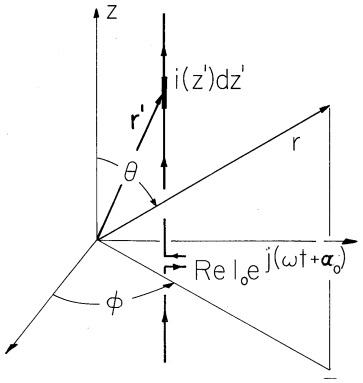


**Fig. 12.4.2** Line current distribution as source of radiation field.

$$\boxed{\hat{E}_\theta \simeq \sqrt{\frac{\mu}{\epsilon}}\hat{H}_\phi} \tag{2}$$

Because **E** and **H** are vector fields, yet another approximation is implicit in writing these expressions. In shifting the current element, there is a slight shift in the coordinate directions at the observer location. Again, because $r$ is much larger than $|\mathbf{r}'|$, this slight change in the direction of the field can be ignored. Thus, radiation fields due to a superposition of current elements can be found by simply superimposing the fields as though they were parallel vectors.

**Distributed Current Distribution.** A wire antenna, driven by a given current distribution Re $[\hat{i}(z)\exp(j\omega t)]$, is shown in Fig. 12.4.2. At the terminals, the complex amplitude of this current is $\hat{i} = I_o \exp(j\omega t + \alpha_o)$. It follows from (1) and the superposition principle that the magnetic radiation field for this antenna is

$$\hat{H}_\phi \simeq \frac{jk}{4\pi}\sin\theta\frac{e^{-jkr}}{r}\int \hat{i}(z')e^{jk\mathbf{r}'\cdot\mathbf{i}_\mathbf{r}}dz' \tag{3}$$

Note that the role played by $id$ for the incremental dipole is now played by $i(z')dz'$. For convenience, we define a field pattern function $\psi_o(\theta)$ that gives the $\theta$ dependence of the $E$ and $H$ fields

$$\boxed{\psi_o(\theta) \equiv \frac{\sin\theta}{l}\int \frac{\hat{i}(z')}{I_o}e^{j(k\mathbf{r}'\cdot\mathbf{i}_\mathbf{r}-\alpha_o)}dz'} \tag{4}$$

where $l$ is the length of the antenna and $\psi_o(\theta)$ is dimensionless. With the aid of $\psi_o(\theta)$, one may write (3) in the form

$$\boxed{\hat{H}_\phi \simeq \frac{jkl}{4\pi}\frac{e^{-jkr}}{r}I_o e^{j\alpha_o}\psi_o(\theta)} \tag{5}$$

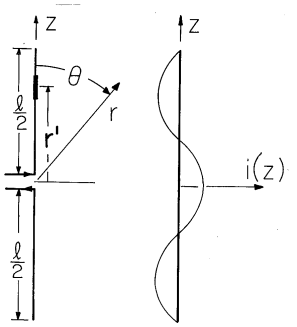


**Fig. 12.4.3** Center-fed wire antenna with standing-wave distribution of current.

By definition, $\hat{i}(\hat{z}') = I_o \exp(j\alpha_o)$ if $z'$ is evaluated at the terminals of the antenna. Thus, $\psi_o$ is neither a function of $I_o$ nor of $\alpha_o$. In order to evaluate (5), one needs to know the current dependence on $z'$, $\hat{i}(z')$. One can show that the current distribution on a (open-ended) thin wire is made up of a "standing wave" with the dependence $\sin(2\pi s/\lambda)$ upon the coordinate $s$ measured along the wire, from the end of the wire. The proof of this statement will be presented in Chapter 14, when we shall discuss the current distribution in a coaxial cable.

**Example 12.4.1.** Radiation Pattern of Center-Fed Wire Antenna

A wire antenna, fed at its midpoint and on the $z$ axis, is shown in Fig. 12.4.3. The current distribution is "given" according to the above remarks.

$$\hat{i} = -I_o \frac{\sin k(|z| - l/2)}{\sin(kl/2)} e^{j\alpha_o} \tag{6}$$

In setting up the radiation field superposition integral, (5), observe that $\mathbf{r}' \cdot \mathbf{i}_\mathbf{r} = z' \cos\theta$.

$$\psi_o = \frac{\sin\theta}{l} \int_{-l/2}^{l/2} \frac{-\sin k(|z'| - l/2)}{\sin(kl/2)} e^{jkz' \cos\theta} dz' \tag{7}$$

Evaluation of the integral[7] then gives

$$\psi_o = \frac{2}{kl \sin(kl/2)} \left[ \frac{\cos(kl/2) - \cos\left(\frac{kl}{2}\cos\theta\right)}{\sin\theta} \right] \tag{8}$$

The radiation pattern of the wire antenna is proportional to the absolute value squared of the $\theta$-dependent factor of $\psi_o$

$$\Psi(\theta) = \left[ \frac{\cos(kl/2) - \cos\left(\frac{kl}{2}\cos\theta\right)}{\sin\theta} \right]^2 \tag{9}$$

[7] To carry out the integration, first express the integration over the positive and negative segments of $z'$ as separate integrals. With the sine functions represented by the sum of complex exponentials, the integration is reduced to a sum of integrations of complex exponentials.

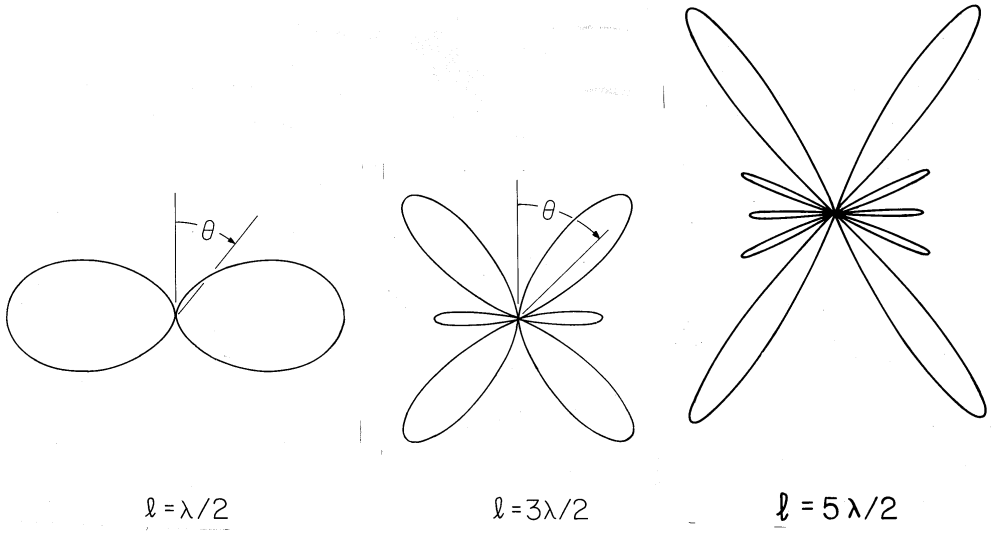


**Fig. 12.4.4** Radiation patterns for center-fed wire antennas.

In viewing the plots of this radiation pattern shown in Fig. 12.4.4, remember that it is the same in any plane of constant $\phi$. Thus, a three-dimensional picture of the function $\Psi(\theta, \phi)$ is generated by rotating one of these patterns about the $z$ axis.

The radiation pattern for a half-wave antenna differs little from that for the short dipole, shown in Fig. 12.2.7. Because of the interference between waves generated by segments having different phases and amplitudes, the pattern for longer wires is more complex. As the length of the antenna is increased to many wavelengths, the number of lobes increases.

**Arrays.** Desired radiation patterns are often obtained by combining driven elements into arrays. To illustrate, consider an array of $1 + n$ elements, the first at the origin and designated by "0". The others are designated by $i = 1 \dots n$ and respectively located at $\mathbf{a}_i$. We can find the radiation pattern for the array by summing over the contributions of the separate elements. Each of these takes the form of (5), with $r \to r - \mathbf{a}_i \cdot \mathbf{i}_\mathbf{r}$, $I_o \to I_i$, $\alpha_o \to \alpha_i$, and $\psi_o(\theta) \to \psi(\theta)$.

$$\hat{H}_\phi \simeq \frac{jkl}{4\pi r} \sum_{i=0}^{n} e^{-jk(r-\mathbf{a}_i \cdot \mathbf{i}_\mathbf{r})} I_i e^{j\alpha_i} \psi_i(\theta) \tag{10}$$

In the special case where the magnitude (but not the phase) of each element is the same and the elements are identical, so that $I_i = I_o$ and $\psi_i = \psi_o$, this expression can be written as

$$\hat{H}_\theta \simeq \frac{jkl}{4\pi} I_o e^{j\alpha_o} \frac{e^{-jkr}}{r} \psi_o(\theta) \psi_a(\theta, \phi) \tag{11}$$

where the *array factor* is

$$\psi_a(\theta, \phi) \equiv \sum_{i=0}^{n} e^{jk\mathbf{a}_i \cdot \mathbf{i}_\mathbf{r}} e^{j(\alpha_i - \alpha_o)} \tag{12}$$

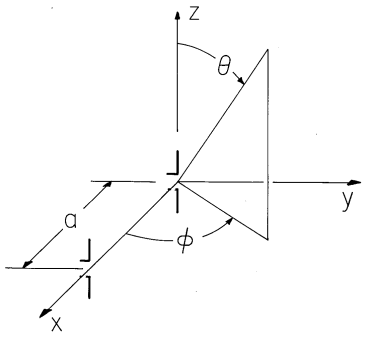


**Fig. 12.4.5** Array consisting of two elements with spacing, $a$.

Note that the radiation pattern of the array is represented by the square of the product of $\psi_o$, representing the pattern for a single element, and the array factor $\psi_a$. If the $n+1$ element array is considered one element in a second array, these same arguments could be repeated to show that the radiation pattern of the array of arrays is represented by the square of the product of $\psi_o$, $\psi_a$ and the square of the array factor of the second array.

**Example 12.4.2.** Two-Element Arrays

The elements of an array have a spacing $a$, as shown in Fig. 12.4.5. The array factor follows from evaluation of (12), where $\mathbf{a}_o = 0$ and $\mathbf{a}_1 = a\mathbf{i}_\mathbf{x}$. The projection of $\mathbf{i}_\mathbf{r}$ into $\mathbf{i}_\mathbf{x}$ gives (see Fig. 12.4.5)

$$\mathbf{a}_1 \cdot \mathbf{i}_\mathbf{r} = a \sin\theta \cos\phi \tag{13}$$

It follows that

$$\psi_a = 1 + e^{j(ka \sin\theta \cos\phi + \alpha_1 - \alpha_o)} \tag{14}$$

It is convenient to write this expression as a product of a part that determines the phase and a part that determines the amplitude.

$$\psi_a = 2e^{j(ka \sin\theta \cos\phi + \alpha_1 - \alpha_o)/2} \cos\left[\frac{ka}{2} \sin\theta \cos\phi + \frac{1}{2}(\alpha_1 - \alpha_o)\right] \tag{15}$$

**Dipoles in Broadside Array.** With the elements short compared to a wavelength, the individual patterns are those of a dipole. It follows from (4) that

$$\psi_o = \sin\theta \tag{16}$$

With the dipoles having a half-wavelength spacing and driven in phase,

$$a = \frac{\lambda}{2} \Rightarrow ka = \pi, \qquad \alpha_1 - \alpha_o = 0 \tag{17}$$

The magnitude of the array factor follows from (15).

$$|\psi_a| = 2\left|\cos\left(\frac{\pi}{2} \sin\theta \cos\phi\right)\right| \tag{18}$$

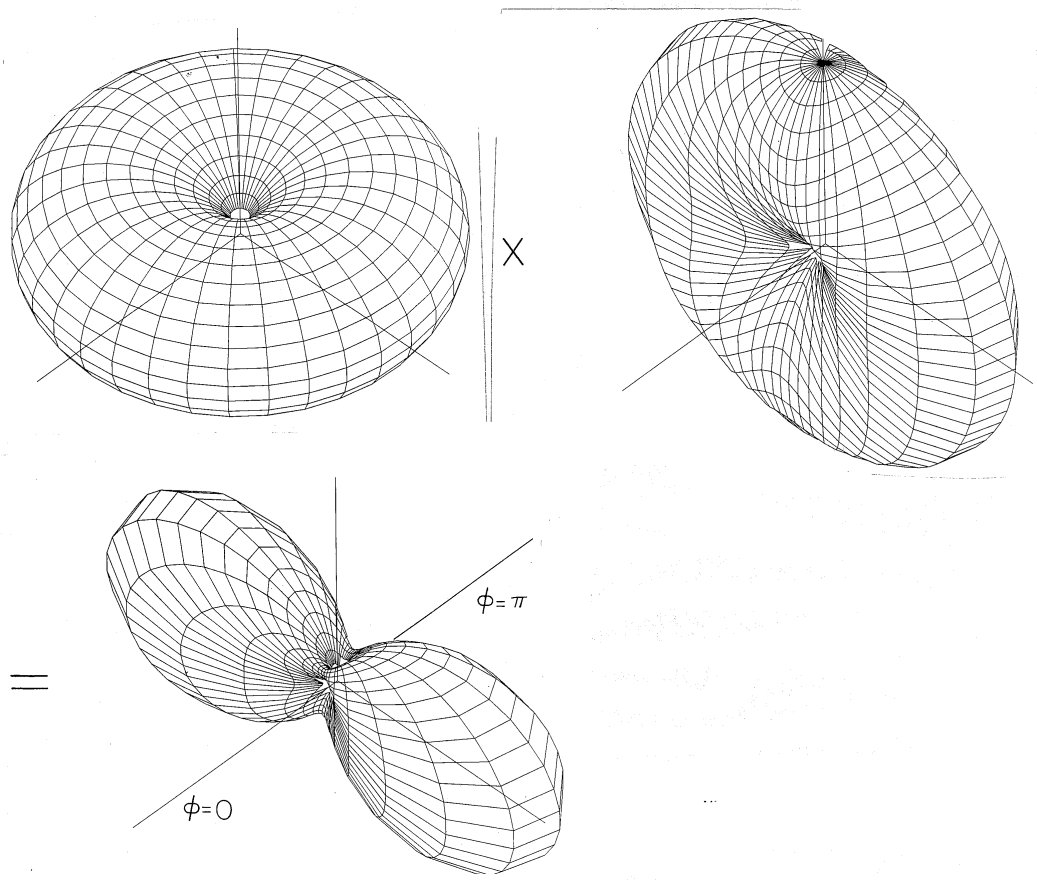


**Fig. 12.4.6** Radiation pattern of dipoles in phase, half-wave spaced, is product of pattern for individual elements multiplied by the array factor.

The radiation pattern for the array follows from (16) and (18).

$$\Psi = |\psi_o|^2 |\psi_a|^2 = 4 \sin^2 \theta \cos^2 \left( \frac{\pi}{2} \sin \theta \cos \phi \right) \tag{19}$$

Figure 12.4.6 geometrically portrays how the single-element pattern and array pattern multiply to provide the radiation pattern. With the elements a half-wavelength apart and driven in phase, electromagnetic waves arrive in phase at points along the $y$ axis and reinforce. There is no radiation in the $\pm x$ directions, because a wave initiated by one element arrives out of phase with the wave being initiated by that second element. As a result, the waves reinforce along the $y$ axis, the "broadside" direction, while they cancel along the $x$ axis.

**Dipoles in End-Fire Array.** With quarter-wave spacing and driven 90 degrees out of phase,

$$a = \frac{\lambda}{4}, \qquad \alpha_1 - \alpha_o = \frac{\pi}{2} \tag{20}$$

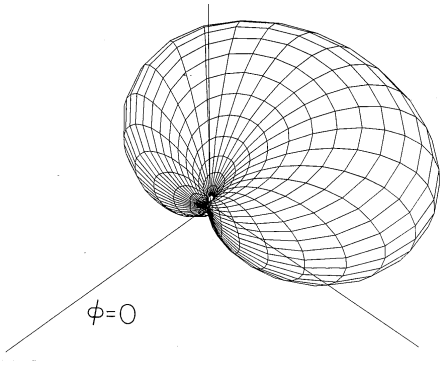


**Fig. 12.4.7** Radiation pattern for dipoles quarter-wave spaced, 90 degrees out of phase.

the magnitude of the array factor follows from (15) as

$$|\psi_a| = 2\Big|\cos\Big[\frac{\pi}{4}\sin\theta\cos\phi + \frac{\pi}{4}\Big]\Big| \tag{21}$$

The radiation pattern follows from (16) and (21).

$$\Psi = |\psi_o|^2|\psi_a|^2 = 4\sin^2\theta\cos^2\Big[\frac{\pi}{4}\sin\theta\cos\phi + \frac{\pi}{4}\Big] \tag{22}$$

Shown graphically in Fig. 12.4.7, the pattern is now in the $-x$ direction. Waves initiated in the $-x$ direction by the element at $x = a$ arrive in phase with those originating from the second element. Thus, the wave being initiated by that second element in the $-x$ direction is reinforced. By contrast, the wave initiated in the $+x$ direction by the element at $x = 0$ arrives 180 degrees out of phase with the wave being initiated in the $+x$ direction by the other element. Thus, radiation in the $+x$ direction cancels, and the array is unidirectional.

**Finite Dipoles in End-Fire Array.** Finally, consider a pair of finite length elements, each having a length $l$, as in Fig. 12.4.3. The pattern for the individual elements is given by (8). With the elements spaced as in Fig. 12.4.5, with $a = \lambda/4$ and driven 90 degrees out of phase, the magnitude of the array factor is given by (21). Thus, the amplitude of the radiation pattern is

$$\Psi = 4\left[\frac{\cos\left(\frac{kl}{2}\right) - \cos\left(\frac{kl}{2}\cos\theta\right)}{\sin\theta}\right]^2\left(\cos^2\Big[\frac{\pi}{4}\sin\theta\cos\phi + \frac{\pi}{4}\Big]\right)^2 \tag{23}$$

For elements of length $l = 3\lambda/2$ ($kl = 3\pi$), this pattern is pictured in Fig. 12.4.8.

**Gain.** The time average power flux density, $\langle S_r(\theta,\ \phi)\rangle$, normalized to the power flux density averaged over the surface of a sphere, is called the *gain* of an antenna.

$$G = \frac{\langle S_r(\theta,\ \phi)\rangle}{\frac{1}{4\pi r^2}\int_0^{\pi}\int_0^{2\pi}\langle S_r\rangle r\sin\theta d\phi r d\theta} \tag{24}$$

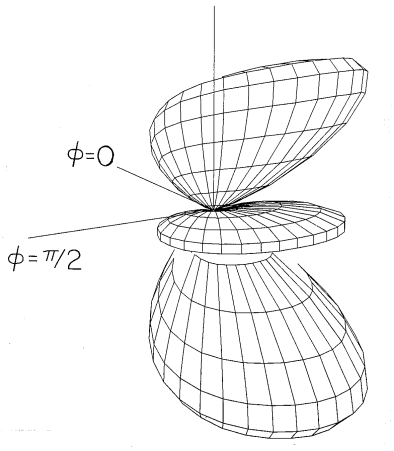


**Fig. 12.4.8** Radiation pattern for two center-fed wire antennas, quarter-wave spaced, 90 degrees out-of-phase, each having length $3\lambda/2$.

If the direction is not specified, it is implied that $G$ is the gain in the direction of maximum gain.

The radial power flux density is the Poynting flux, defined by (11.2.9). Using the time average theorem, (11.5.6), and the fact that the ratio of $\mathbf{E}$ to $\mathbf{H}$ for the radiation field is $\sqrt{\mu/\epsilon}$, (2), gives

$$\langle S_r \rangle = \frac{1}{2} Re\hat{\mathbf{E}} \times \hat{\mathbf{H}}^* = \frac{1}{2} Re\hat{E}_\theta \hat{H}_\phi^* = \frac{1}{2}\sqrt{\epsilon/\mu}|\hat{E}_\theta|^2 \tag{25}$$

Because the radiation pattern expresses the $(\theta,\ \phi)$ dependence of $|E_\theta|^2$ with a multiplicative factor that is in common to the numerator and denominator of (24), $G$ can be evaluated using the radiation pattern $\Psi$ for $\langle S_r \rangle$.

**Example 12.4.3.** Gain of an Electric Dipole

For the electric dipole, it follows from (1) and (2) that the radiation pattern is proportional to $\sin^2(\theta)$. The gain in the $\theta$ direction is then

$$G = \frac{\sin^2\theta}{\frac{1}{2}\int_0^\pi \sin^3\theta d\theta} = \frac{3}{2}\sin^2\theta \tag{26}$$

and the "gain" is 3/2.

## 12.5 COMPLEX POYNTING'S THEOREM AND RADIATION RESISTANCE

To the generator supplying its terminal current, a radiating antenna appears as a load with an impedance having a resistive part. This is true even if the antenna is made from perfectly conducting material and therefore incapable of converting

electrical power to heat. The power radiated away from the antenna must be supplied through its terminals, much as if it were dissipated in a resistor. Indeed, if there is no electrical dissipation in the antenna, the power supplied at the terminals is that radiated away. This statement of power conservation makes it possible to determine the equivalent resistance of the antenna simply by using the far fields that were the theme of Sec. 12.4.

**Complex Poynting's Theorem.** For systems in the sinusoidal steady state, a useful alternative to the form of Poynting's theorem introduced in Secs. 11.1 and 11.2 results from writing Maxwell's equations in terms of complex amplitudes *before* they are combined to provide the desired theorem. That is, we assume at the outset that fields and sources take the form

$$\mathbf{E} = Re\hat{\mathbf{E}}(x,y,z)e^{j\omega t} \tag{1}$$

Suppose that the region of interest is composed either of free space or of perfect conductors. Then, substitution of complex amplitudes into the laws of Ampère and Faraday, (12.0.8) and (12.0.9), gives

$$\nabla \times \hat{\mathbf{H}} = \hat{\mathbf{J}} + j\omega\epsilon\hat{\mathbf{E}} \tag{2}$$

$$\nabla \times \hat{\mathbf{E}} = -j\omega\mu\hat{\mathbf{H}} \tag{3}$$

The manipulations that are now used to obtain the desired "complex Poynting's theorem" parallel those used to derive the real, time-dependent form of Poynting's theorem in Sec. 11.2. We *dot* $\mathbf{E}$ with the complex conjugate of (2) and subtract the dot product of the complex conjugate of $\mathbf{H}$ with (3). It follows that[8]

$$-\nabla \cdot (\hat{\mathbf{E}} \times \hat{\mathbf{H}}^*) = \hat{\mathbf{E}} \cdot \hat{\mathbf{J}}^* + j\omega(\mu\hat{\mathbf{H}} \cdot \hat{\mathbf{H}}^* - \epsilon\hat{\mathbf{E}} \cdot \hat{\mathbf{E}}^*) \tag{4}$$

The object of this manipulation was to obtain the "perfect" divergence on the left, because this expression can then be integrated over a volume $V$ and Gauss' theorem used to convert the volume integral on the left to an integral over the enclosing surface $S$.

$$\begin{aligned} -\oint_S \frac{1}{2}(\hat{\mathbf{E}} \times \hat{\mathbf{H}}^*) \cdot d\mathbf{a} = & j\omega 2 \int_V \frac{1}{4}(\mu\hat{\mathbf{H}} \cdot \hat{\mathbf{H}}^* - \epsilon\hat{\mathbf{E}} \cdot \hat{\mathbf{E}}^*)dv \\ & + \int_V \frac{1}{2}\hat{\mathbf{E}} \cdot \hat{\mathbf{J}}_u^* dv \end{aligned} \tag{5}$$

This expression has been multiplied by $\frac{1}{2}$, so that its real part represents the time average flow of power, familiar from Sec. 11.5. Note that the real part of the first term on the right is zero. The real part of (5) equates the time average of the Poynting vector flux into the volume with the time average of the power imparted to the current density of unpaired charge, $\mathbf{J}_u$, by the electric field. This information

[8] $\nabla \cdot (\mathbf{A} \times \mathbf{B}) = \mathbf{B} \cdot \nabla \times \mathbf{A} - \mathbf{A} \cdot \nabla \times \mathbf{B}$

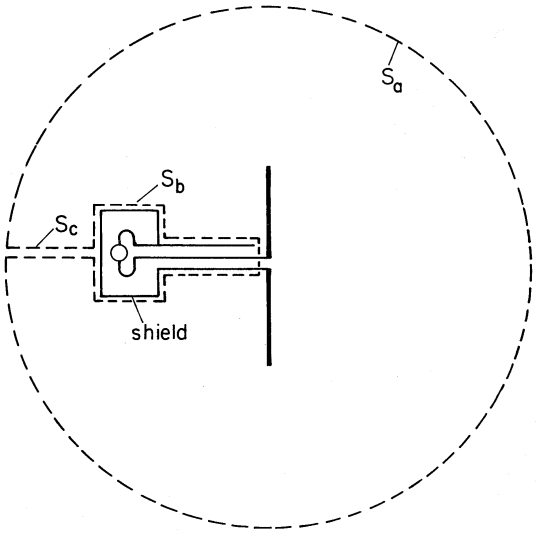


**Fig. 12.5.1** Surface $S$ encloses the antenna but excludes the source. Spherical part of $S$ is at "infinity."

is equivalent to the time average of the (real form of) Poynting's theorem. The imaginary part of (5) relates the difference between the time average magnetic and electric energies in the volume $V$ to the imaginary part of the complex Poynting flux into the volume. The imaginary part of the complex Poynting theorem conveys additional information.

**Radiation Resistance.** Consider the perfectly conducting antenna system surrounded by the spherical surface, $S$, shown in Fig. 12.5.1. To exclude sources from the enclosed volume, this surface is composed of an outer surface, $S_a$, that is far enough from the antenna so that only the radiation field makes a contribution, a surface $S_b$ that surrounds the source(s), and a surface $S_c$ that can be envisioned as the wall of a system of thin tubes connecting $S_a$ to $S_b$ in such a way that $S_a + S_b + S_c$ is indeed the surface enclosing $V$. By making the connecting tubes very thin, contributions to the integral on the left in (5) from the surface $S_c$ are negligible. We now write, and then explain, the terms in (5) as they describe this radiation system.

$$-\int_{S_a} \frac{1}{2}\sqrt{\epsilon/\mu}|\hat{E}_\theta|^2 da + \sum_{i=1}^{n} \frac{1}{2}\hat{v}_i\hat{i}_i^* = j2\omega \int_V \frac{1}{2}\left(\frac{1}{2}\mu|\hat{\mathbf{H}}|^2 - \frac{1}{2}\epsilon|\hat{\mathbf{E}}|^2\right)dv \qquad (6)$$

The first term is the contribution from integrating the radiation Poynting flux over $S_a$, where (12.4.2) serves to eliminate $\mathbf{H}$. The second term comes from the surface integral in (5) of the Poynting flux over the surface, $S_b$, enclosing the sources (generators). Think of the generators as enclosed by perfectly conducting boxes powered by terminal pairs (coaxial cables) to which the antennae are attached. We have shown in Sec. 11.3 (11.3.29) that the integral of the Poynting flux over $S_b$ is

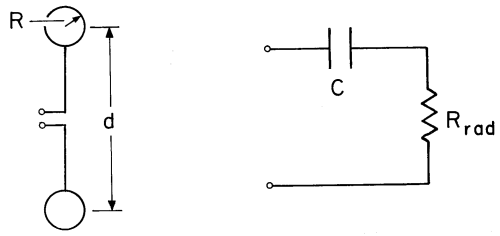


**Fig. 12.5.2** End-loaded dipole and equivalent circuit.

equivalent to the sum of voltage-current products expressing power flow from the circuit point of view. The first term on the right is the same as the first on the right in (5). Finally, the last term in (5) makes no contribution, because the only regions where $\mathbf{J}$ exists within $V$ are those modeled here as perfectly conducting and hence where $\mathbf{E} = 0$.

Consider a single antenna with one input terminal pair. The antenna is a linear system, so the complex voltage must be proportional to the complex terminal current.

$$\hat{v} = Z_{\text{ant}}\hat{i} \tag{7}$$

Here, $Z_{\text{ant}}$ is the impedance of the antenna. In terms of this impedance, the time average power can be written as

$$\frac{1}{2}Re(\hat{v}\hat{i}^*) = \frac{1}{2}Re(Z_{\text{ant}})|\hat{i}|^2 = \frac{1}{2}Re(Z_{\text{ant}})|\hat{I}_o|^2 \tag{8}$$

It follows from the real part of (6) that the *radiation resistance*, $R_{\text{rad}}$, is

$$Re(Z_{\text{ant}}) \equiv R_{\text{rad}} = \sqrt{\epsilon/\mu}\int_{S_a}|E_\theta|^2\frac{da}{|\hat{I}_o|^2} \tag{9}$$

The imaginary part of $Z_{\text{out}}$ describes the reactive power supplied to the antenna.

$$Im(Z_{\text{ant}}) = \frac{\omega\int(\mu|\hat{\mathbf{H}}|^2 - \epsilon|\hat{\mathbf{E}}|^2)dv}{|I_o|^2} \tag{10}$$

The radiation field contributions to this integral cancel out. If the antenna elements are short compared to a wavelength, contributions to (10) are dominated by the quasistatic fields. Thus, the electric dipole contributions are dominated by the electric field (and the reactance is capacitive), while those for the magnetic dipole are inductive. By making the antenna on the order of a wavelength, the magnetic and electric contributions to (10) are often made to essentially cancel. An example is a half-wavelength version of the wire antenna in Example 12.4.1. The equivalent circuit for such resonant antennae is then solely the radiation resistance.

**Example 12.5.1.** Equivalent Circuit of an Electric Dipole

An "end-loaded" electric dipole is composed of a pair of perfectly conducting metal spheres, each of radius $R$, as shown in Fig. 12.5.2. These spheres have a spacing, $d$, that is short compared to a wavelength but large compared to the radius, $R$, of the spheres.

The equivalent circuit is also shown in Fig. 12.5.2. The statement that the sum of the voltage drops around the circuit is zero requires that

$$\hat{v} = \frac{\hat{i}}{j\omega C} + R_{\rm rad}\hat{i} \tag{11}$$

A statement of power flow is obtained by multiplying this expression by the complex conjugate of the complex amplitude of the current.

$$\frac{1}{2}\hat{v}\hat{i}^* = -\frac{j\omega}{2C}\hat{q}\hat{q}^* + \frac{1}{2}R_{\rm rad}\hat{i}\hat{i}^*; \qquad \hat{i} \equiv j\omega\hat{q} \tag{12}$$

Here the dipole charge, $q$, is defined such that $i = dq/dt$. The real part of this expression takes the same form as the statement of complex power flow for the antenna, (6). Thus, with $\hat{E}_\theta$ provided by (12.2.23) and (12.2.24), we can solve for the radiation resistance:

$$R_{\rm rad} = \sqrt{\mu/\epsilon}\frac{(kd)^2}{(4\pi)^2}\int_0^\pi \frac{\sin^2\theta(2\pi r\sin\theta)rd\theta}{r^2} = \frac{(kd)^2}{6\pi}\sqrt{\mu/\epsilon} \tag{13}$$

Note that because $k \equiv \omega/c$, this radiation resistance is proportional to the square of the frequency.

The imaginary part of the impedance is given by the right-hand side of (10). The radiation field contributions to this integral cancel out. In integrating over the near field, the electric energy storage dominates and becomes essentially that associated with the quasistatic capacitance of the pair of spheres. We assume that the spheres are connected by wires that are extremely thin, so that their effect can be ignored. Then, the capacitance is the series capacitance of two isolated spheres, each having a capacitance of $4\pi\epsilon R$.

$$C = 2\pi\epsilon R \tag{14}$$

Radiation fields are solutions to the full Maxwell equations. In contrast, EQS fields were analyzed ignoring the magnetic flux linkage in Faraday's law. The approximation is justified if the size of the system is small compared with a wavelength. The following example treats the scattering of particles that are small compared with the wavelength. The fields around the particles are EQS, and the currents induced in the particles are deduced from the EQS approximation. These currents drive radiation fields, resulting in Rayleigh scattering. The theory of Rayleigh scattering explains why the sky is blue in color, as the following example shows.

**Example 12.5.2.** Rayleigh Scattering

Consider a spatial distribution of particles in the field of an infinite parallel plane wave. The particles are assumed to be small as compared to the wavelength of the plane wave. They get polarized in the presence of an electric field $\mathbf{E}_a$, acquiring a dipole moment

$$\mathbf{p} = \epsilon_o\alpha\mathbf{E}_a \tag{15}$$

where $\alpha$ is the polarizability. These particles could be atoms or molecules, such as the molecules of nitrogen and oxygen of air exposed to visible light. They could also

be conducting spheres of radius $R$. In the latter case, the dipole moment produced by an applied electric field $E_a$ is given by (6.6.5) and the polarizability is

$$\alpha = 4\pi R^3 \tag{16}$$

If the frequency of the polarizing wave is $\omega$ and its propagation constant $k = \omega/c$, the far field radiated by the particle, expressed in a spherical coordinate system with its $\theta = 0$ axis aligned with the electric field of the wave, is, from (12.2.22),

$$E_\theta = -\sqrt{\frac{\mu_o}{\epsilon_o}}\frac{k\omega\hat{p}}{4\pi}\sin\theta\frac{e^{-jkr}}{r} \tag{17}$$

where $\hat{i}d = j\omega\hat{p}$ is used in the above expression. The power radiated by each dipole, i.e., the power scattered by a dipole, is

$$\begin{aligned} P_{\text{Scatt}} &= \int_{S_a}\frac{1}{2}\sqrt{\frac{\epsilon_o}{\mu_o}}|\hat{E}_\theta|^2 = \frac{1}{2}\sqrt{\frac{\mu_o}{\epsilon_o}}\left|\frac{\omega k\hat{p}}{4\pi}\right|^2\frac{1}{r^2}\int_0^\pi\int_0^{2\pi} d\phi r^2\sin^3\theta d\theta \\ &= \frac{1}{2}\sqrt{\frac{\mu_o}{\epsilon_o}}\left|\frac{\omega k\hat{p}}{4\pi}\right|^2\frac{8\pi}{3} = \frac{1}{12\pi}\sqrt{\frac{\mu_o}{\epsilon_o}}\frac{\omega^4}{c^2}\epsilon_o^2\alpha^2\hat{\mathbf{E}}^2 \end{aligned} \tag{18}$$

The scattered power increases with the fourth power of frequency when $\alpha$ is not a function of frequency. The polarizability of $N_2$ and $O_2$ is roughly frequency independent. Of the visible radiation, the blue (high) frequencies scatter much more than the red (low) frequencies. This is the reason for the blue color of the sky. The same phenomenon accounts for the polarization of the scattered radiation. Along a line $L$ at a large angle from the line from the observer $O$ to the sun $S$, only the electric field perpendicular to the plane $LOS$ produces radiation visible at the observer position (note the $\sin^2\theta$ dependence of the radiation). Thus, the scattered radiation observed at $O$ has an electric field perpendicular to $LOS$.

The present analysis has made two approximations. First, of course, we assumed that the particle is small compared with a wavelength. Second, we computed the induced polarization from the unperturbed field $E_\theta$ of the incident plane wave. This assumes that the particle perturbs the wave negligibly, that the scattered power is very small compared to the power in the wave. Of course, the incident wave decreases in intensity as it proceeds through the distribution of scatterers, but this macroscopic change can be treated as a simple attenuation proportional to the density of scatterers.

## 12.6 PERIODIC SHEET-SOURCE FIELDS: UNIFORM AND NONUNIFORM PLANE WAVES

This section introduces the electrodynamic fields associated with surface sources. The physical systems analyzed are generalizations, on the one hand, of such EQS situations as Example 5.6.2, where sinusoidal surface charge densities produced a Laplacian field decaying away from the surface charge source. On the other hand, the MQS sinusoidal surface current sources producing magnetic fields that decay

away from their source (for example, Prob. 8.6.9) are generalized to the fully dynamic case. In both cases, one expects that the quasistatic approximation will be contained in the limit where the spatial period of the source is much smaller than the wavelength $\lambda = 2\pi/\omega\sqrt{\mu\epsilon}$. When the spatial period of the source approaches, or exceeds, the wavelength, new phenomena ought to be revealed. Specifically, distributions of surface current density $\mathbf{K}$ and surface charge density $\sigma_s$ are given in the $x-z$ plane.

$$\mathbf{K} = K_x(x,t)\mathbf{i_x} + K_z(x,t)\mathbf{i_z} \tag{1}$$

$$\sigma_s = \sigma_s(x,t) \tag{2}$$

These are independent of $z$ and are typically periodic in space and time, extending to infinity in the $x$ and $z$ directions.

Charge conservation links $\mathbf{K}$ and $\sigma_s$. A two-dimensional version of the charge conservation law, (12.1.22), requires that there must be a time rate of decrease of surface charge density $\sigma_s$ wherever there is a two-dimensional divergence of $\mathbf{K}$.

$$\frac{\partial K_x}{\partial x} + \frac{\partial K_z}{\partial z} + \frac{\partial \sigma_s}{\partial t} = 0 \Rightarrow \frac{\partial K_x}{\partial x} + \frac{\partial \sigma_s}{\partial t} = 0 \tag{3}$$

The second expression results because $K_z$ is independent of $z$.

Under the assumption that the only sources are those in the $x-z$ plane, it follows that the fields can be pictured as the superposition of those due to $(K_x, \sigma_s)$ given to satisfy (3) and due to $K_z$. It is therefore convenient to break the fields produced by these two kinds of sources into two categories.

**Transverse Magnetic (TM) Fields.** The source distribution $(K_x, \sigma_s)$ does not produce a $z$ component of the vector potential $\mathbf{A}$, $A_z = 0$. This follows because there is no $z$ component of the current in the superposition integral for $\mathbf{A}$, (12.3.2). However, there are both current and charge sources, so that the superposition integral for $\Phi$ requires that in addition to an $\mathbf{A}$ that lies in $x-y$ planes, there is an electric potential as well.

$$\mathbf{A} = A_x(x,y,t)\mathbf{i_x} + A_y(x,y,t)\mathbf{i_y}; \qquad \Phi = \Phi(x,y,t) \tag{4}$$

Because the source distribution is independent of $z$, we have taken these potentials to be also two dimensional. It follows that $\mathbf{H}$ *is transverse to the* $x-y$ *coordinates upon which the fields depend*, while $\mathbf{E}$ lies in the $x-y$ plane.

$$\mathbf{H} = \frac{1}{\mu}\nabla \times \mathbf{A} = H_z(x,y,t)\mathbf{i_z}$$

$$\mathbf{E} = -\nabla\Phi - \frac{\partial \mathbf{A}}{\partial t} = E_x(x,y,t)\mathbf{i_x} + E_y(x,y,t)\mathbf{i_y} \tag{5}$$

Sources and fields for these transverse magnetic (TM) fields have the relative orientations shown in Fig. 12.6.1.

We will be concerned here with sources that are in the sinusoidal steady state. Although $\mathbf{A}$ and $\Phi$ could be used to derive the fields, in what follows it is more

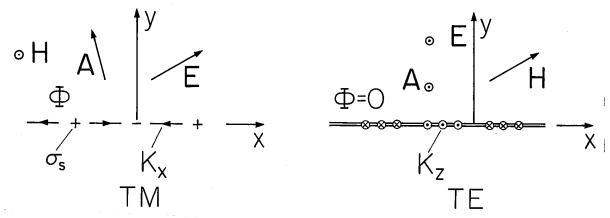


**Fig. 12.6.1** Transverse magnetic and electric sources and fields.

convenient to deal directly with the fields themselves. The complex amplitude of $H_z$, the only component of $\mathbf{H}$, is conveniently used to represent $\mathbf{E}$ in the free space regions to either side of the sheet. This can be seen by using the $x$ and $y$ components of Ampère's law to write

$$\boxed{E_x = \frac{1}{j\omega\epsilon}\frac{\partial \hat{H}_z}{\partial y}} \tag{6}$$

$$\boxed{\hat{E}_y = -\frac{1}{j\omega\epsilon}\frac{\partial \hat{H}_z}{\partial x}} \tag{7}$$

for the only two components of $\mathbf{E}$.

The relationship between $\mathbf{H}$ and its source is obtained by taking the curl of the vector wave equation for $\mathbf{A}$, (12.1.8). The curl operator commutes with the Laplacian and time derivative, so that the result is the inhomogeneous wave equation for $\mathbf{H}$.

$$\boxed{\nabla^2\mathbf{H} - \mu\epsilon\frac{\partial^2\mathbf{H}}{\partial t^2} = -\nabla\times\mathbf{J}} \tag{8}$$

For the sheet source, the driving term on the right is zero everywhere except in the $x-z$ plane. Thus, in the free space regions, the $z$ component of this equation gives a differential equation for the complex amplitude of $H_z$.

$$\boxed{(\frac{\partial^2}{\partial x^2} + \frac{\partial^2}{\partial y^2})\hat{H}_z + \omega^2\mu\epsilon\hat{H}_z = 0} \tag{9}$$

This expression is a two-dimensional example of the *Helmholtz equation.* Given sinusoidal steady state source distributions of $(K_x, \sigma_s)$ consistent with charge conservation, (3), the continuity conditions can be used to relate these sources to the fields described by (6), (7), and (9).

**Product Solutions to the Helmholtz Equation.** One theme of this section is the solution to the Helmholtz equation, (9). Note that this equation resulted from the time-dependent wave equation by separation of variables, by assuming solutions of the form $H_z(x,y)T(t)$, where $T(t) = \exp(j\omega t)$. We now look for solutions expressing the $x-y$ dependence that take the product form $X(x)Y(y)$. The process is familiar from Sec. 5.4, but the resulting family of solutions is of wider variety, and it is worthwhile to focus on their nature before applying them to particular examples.

With the substitution of the product solution $H_z = X(x)Y(y)$, (9) becomes

$$\frac{1}{X}\frac{d^2X}{dx^2} + \frac{1}{Y}\frac{d^2Y}{dy^2} + \omega^2\mu\epsilon = 0 \tag{10}$$

This expression is satisfied if the first and second terms are constants

$$-k_x^2 - k_y^2 + \omega^2\mu\epsilon = 0 \tag{11}$$

and it follows that parts of the total solution are governed by the ordinary differential equations

$$\frac{d^2X}{dx^2} + k_x^2 X = 0; \qquad \frac{d^2Y}{dy^2} + k_y^2 Y = 0. \tag{12}$$

Although $k_x$ and $k_y$ are constants, as long as they satisfy (11) they can be real or imaginary. In this chapter, we are interested in solutions that are periodic in the $x$ direction, so we can think of $k_x$ as being real and $k_x^2 > 0$. Furthermore, the value of $k_x$ is fixed by the assumed functional form of the surface currents and charges. Equation (11) then determines $k_y$ from given values of $k_x$ and $\omega$. In solving (11) for $k_y$, we must take the square root of a quantity that can be positive or negative. By way of distinguishing the two roots of (11) solved for $k_y$, we define

$$\boxed{\beta \equiv \begin{cases} |\sqrt{\omega^2\mu\epsilon - k_x^2}|; & \omega^2\mu\epsilon > k_x^2 \\ -j|\sqrt{k_x^2 - \omega^2\mu\epsilon}|; & \omega^2\mu\epsilon < k_x^2 \end{cases}} \tag{13}$$

and write the two solutions to (11) as

$$k_y \equiv \mp\beta \tag{14}$$

Thus, $\beta$ is defined as either positive real or negative imaginary, and what we have found for the product solution $X(x)Y(y)$ are combinations of products

$$\hat{H}_z\alpha \left\{ \begin{matrix} \cos k_x x \\ \sin k_x x \end{matrix} \right\} \left\{ \begin{matrix} e^{-j\beta y} \\ e^{j\beta y} \end{matrix} \right\} \tag{15}$$

Note that if $\omega^2\mu\epsilon < k_x^2$, $k_y$ is defined by (13) and (14) such that the field, which is periodic in the $x$ direction, decays in the $+y$ direction for the upper solution but decays in the $-y$ direction for the lower solution. These fields resemble solutions to

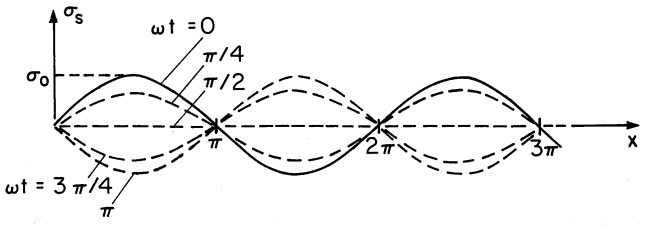


**Fig. 12.6.2** Standing wave of surface charge density.

Laplace's equation. Indeed, in the limit where $\omega^2\mu\epsilon \ll k_x^2$, the Helmholtz equation becomes Laplace's equation.

As the frequency is raised, the rate of decay in the $\pm y$ directions decreases until $k_y$ becomes real, at which point the solutions take a form that is in sharp contrast to those for Laplace's equation. With $\omega^2\mu\epsilon > k_x^2$, the solutions that we assumed to be periodic in the $x$ direction are *also periodic in the y direction.*

The wave propagation in the $y$ direction that renders the solutions periodic in $y$ is more evident if the product solutions of (15) are written with the time dependence included.

$$H_z \,\alpha \left\{ \begin{matrix} \cos k_x x \\ \sin k_x x \end{matrix} \right\} e^{j(\omega t \mp \beta y)} \tag{16}$$

For $\omega^2\mu\epsilon > k_x^2$, the upper and lower signs in (16) [and hence in (14)] correspond to waves propagating in the positive and negative $y$ directions, respectively.

By taking a linear combination of the trigonometric functions in (16), we can also form the complex exponential $\exp(jk_x x)$. Thus, another expression of the solutions given by (16) is as

$$H_z \,\alpha\, e^{j(\omega t \mp \beta y \mp k_x x)} \tag{17}$$

Instead of having standing waves in the $x$ direction, as represented by (16), we now have solutions that are traveling in the $\pm x$ directions. Examples 12.6.1 and 12.6.2, respectively, illustrate how standing-wave and traveling-wave fields are excited.

**Example 12.6.1.** Standing-Wave TM Fields

Consider the field response to a surface charge density that is in the sinusoidal steady state and represented by

$$\sigma_s = Re\left[\hat{\sigma}_o \sin k_x x e^{j\omega t}\right] \tag{18}$$

The complex coefficient $\hat{\sigma}_o$, which determines the temporal phase and magnitude of the charge density at any given location $x$, is given. Figure 12.6.2 shows this function represented in space and time. The charge density is always zero at the locations $k_x x = n\pi$, where $n$ is any integer, and oscillates between positive and negative peak amplitudes at locations in between. When it is positive in one half-period between nulls, it is negative in the adjacent half-periods. It has the $x$ dependence of a standing wave.

The current density that is consistent with the surface charge density of (18) follows from (3).

$$K_x = Re\left[\frac{j\omega\hat{\sigma}_o}{k_x}\cos k_x x e^{j\omega t}\right] \tag{19}$$

With the surface current density in the $z$ direction zero, the fields excited by these surface sources above and below the sheet are TM. The continuity conditions, (12.1.14)–(12.1.17), relate the fields to the given surface source distributions.

We start with Ampère's continuity condition, the $x$ component of (12.1.15)

$$H_z^a - H_z^b = K_x \quad \text{at} \quad y = 0 \tag{20}$$

because it determines the $x$ dependence of $H_z$ as $\cos k_x x$. Of the possible combinations of solutions given by (15), we let

$$\hat{H}_z = \begin{cases} \hat{A}\cos k_x x e^{-j\beta y} \\ \hat{B}\cos k_x x e^{j\beta y} \end{cases} \tag{21}$$

The upper solution pertains to the upper region. Note that we select a $y$ dependence that represents either a wave propagating in the $+y$ direction (for $\omega^2\mu\epsilon > 0$) or a field that decays in that direction (for $\omega^2\mu\epsilon < 0$). The lower solution, which applies in the lower region, either propagates in the $-y$ direction or decays in that direction. One of two conditions on the coefficients in (21) it follows from substitution of these equations into Ampère's continuity condition, (20).

$$\hat{A} - \hat{B} = \frac{j\omega\hat{\sigma}_o}{k_x} \tag{22}$$

A second condition follows from Faraday's continuity condition, (12.1.16), which requires that the tangential electric field be continuous.

$$\hat{E}_x^a - \hat{E}_x^b = 0 \quad \text{at} \quad y = 0 \tag{23}$$

Substitution of the solutions, (21), into (6) gives $\hat{E}_x^a$ and $\hat{E}_x^b$, from which follows

$$\hat{A} = -\hat{B} \tag{24}$$

Combining (2) and (3) we find

$$\hat{A} = -\hat{B} = \frac{j\omega\hat{\sigma}_o}{2k_x} \tag{25}$$

The remaining continuity conditions are now automatically satisfied. There is no normal flux density, so the flux continuity condition of (12.1.17) is automatically satisfied. But even if there were a $y$ component of $\mathbf{H}$, continuity of tangential $\mathbf{E}$ as expressed by (23) would guarantee that this condition is satisfied.

In summary, the coefficients given by (25) can be used in (21), and those expressions introduced into (6) and (7), to determine the fields as

$$H_z = Re \pm \frac{j\omega\hat{\sigma}_o}{2k_x}\cos k_x x e^{j(\omega t \mp \beta y)} \tag{26}$$

$$E_x = Re - \frac{j\hat{\sigma}_o\beta}{2\epsilon k_x}\cos k_x x e^{j(\omega t \mp \beta y)} \tag{27}$$

$$E_y = Re \pm \frac{\hat{\sigma}_o}{2\epsilon}\sin k_x x e^{j(\omega t \mp \beta y)} \tag{28}$$

These fields are pictured in Fig. 12.6.3 for the case where $\sigma_o$ is real. In the first field distribution, the frequency is low enough so that $\omega^2\mu\epsilon < k_x^2$. Thus, $\beta$ as given by (13) has a negative imaginary value. The electric field pattern is shown when $t = 0$. At this instant, $\mathbf{H} = 0$. When $\omega t = \pi/2$, $\mathbf{H}$ is as shown while $\mathbf{E} = 0$. The $\mathbf{E}$ and $\mathbf{H}$ are 90 degrees out of temporal phase. The fields decay in the $y$ direction, much as they would for a spatially periodic surface charge distribution in the EQS limit. Because they decay in the $\pm y$ directions for reasons that do not involve dissipation, these fields are sometimes called *evanescent waves*. The decay has its origins in the nature of quasistatic fields, shaped as they are by Laplace's equation. Indeed, with $\omega^2\mu\epsilon \ll k_x^2$, $\mathbf{E} = -\nabla\Phi$, and we are dealing with scalar solutions $\Phi$ to Laplace's equation. The field pattern corresponds to that of Example 5.6.2. As the frequency is raised, the rate of decay in the $y$ direction decreases. The rate of decay, $|\beta|$, reaches zero as the frequency reaches $\omega = k_x/\sqrt{\mu\epsilon} = k_x c$. The physical significance of this condition is seen by recognizing that $k_x = 2\pi/\lambda_x$, where $\lambda_x$ is the wavelength in the $x$ direction of the imposed surface charge density, and that $\omega = 2\pi/T$ where $T$ is the temporal period of the excitation. Thus, as the frequency is raised to the point where the fields no longer decay in the $\pm y$ directions, the period $T$ has become $T = \lambda_x/c$, and so has become as short as the time required for an electromagnetic wave to propagate the wavelength $\lambda_x$.

The second distribution of Fig. 12.6.3 illustrates what happens to the fields as the frequency is raised beyond the cutoff frequency, when $\omega^2\mu\epsilon > k_x^2$. In this case, both $\mathbf{E}$ and $\mathbf{H}$ are shown in Fig. 12.6.3 when $t = 0$. Fields above and below the sheet propagate in the $\pm y$ directions, respectively. As time progresses, the evolution of the fields in the respective regions can be pictured as a translation of these distributions in the $\pm y$ directions with the phase velocities $\omega/k_y$.

**Transverse Electric (TE) Fields.** Consider the case of a $z$-directed surface current density $\mathbf{K} = k_z\mathbf{i_z}$. Then, the surface charge density $\sigma_s$ is zero. It follows from the superposition integral for $\Phi$, (12.3.1), that $\Phi = 0$ and from the superposition integral for $\mathbf{A}$, (12.3.2), that $\mathbf{A} = A_z\mathbf{i_z}$. Equation (12.1.3) then shows that $\mathbf{E}$ is in the $z$ direction, $\mathbf{E} = E_z\mathbf{i_z}$. *The electric field is transverse to the $x$ and $y$ axes*, while the magnetic field lines are in $x - y$ planes. These are the field directions summarized in the second part of Fig. 12.6.1.

In the sinusoidal steady state, it is convenient to use $E_z$ as the function from which all other quantities can be derived, for it follows from Faraday's law that the two components of $\mathbf{H}$ can be written in terms of $E_z$.

$$\boxed{\hat{H}_x = -\frac{1}{j\omega\mu}\frac{\partial\hat{E}_z}{\partial y}} \tag{29}$$

$$\boxed{\hat{H}_y = \frac{1}{j\omega\mu}\frac{\partial\hat{E}_z}{\partial x}} \tag{30}$$

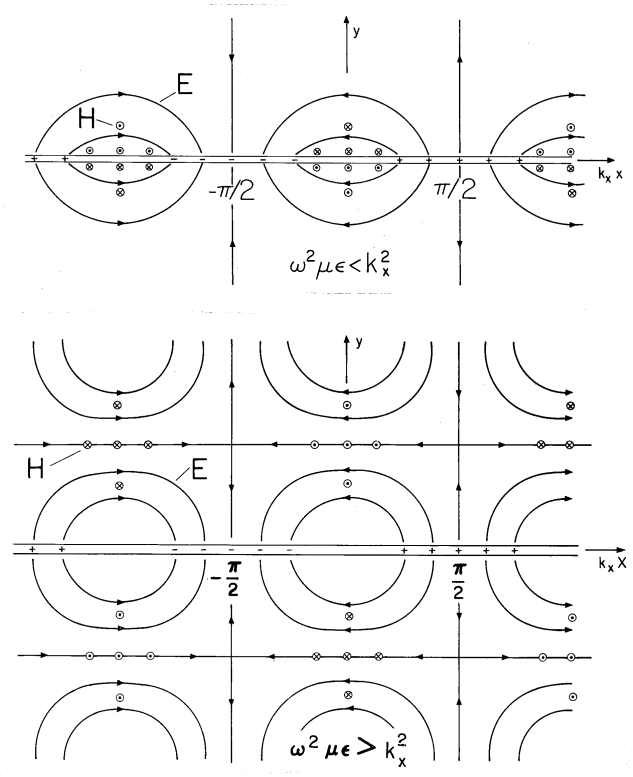


**Fig. 12.6.3** TM waves due to standing wave of sources in $y = 0$ plane.

In the free space regions to either side of the sheet, each of the Cartesian components of $\mathbf{E}$ and $\mathbf{H}$ satisfies the wave equation. We have already seen this for $\mathbf{H}$. To obtain an expression playing a similar role for $\mathbf{E}$, we could again return to the wave equations for $\mathbf{A}$ and $\Phi$. A more direct derivation begins by taking the curl of Faraday's law.

$$\nabla \times \nabla \times \mathbf{E} = -\nabla \times \frac{\partial \mu \mathbf{H}}{\partial t} \Rightarrow \nabla(\nabla \cdot \mathbf{E}) - \nabla^2 \mathbf{E} = -\mu \frac{\partial}{\partial t}(\nabla \times \mathbf{H}) \tag{31}$$

On the left, a vector identity has been used, while on the right the order of taking the time derivative and the curl has been reversed. Now, if we substitute for the divergence on the left using Gauss' law, and for the curl on the right using Ampère's law, it follows that

$$\boxed{\nabla^2 \mathbf{E} - \mu\epsilon \frac{\partial^2 \mathbf{E}}{\partial t^2} = \nabla\left(\frac{\rho}{\epsilon}\right) + \mu \frac{\partial \mathbf{J}}{\partial t}} \tag{32}$$

In the free space regions, the driving terms on the right are absent. In the case of transverse electric fields, $\hat{E}_z$ is the only field component. From (32), an assumed

time dependence of the form $\mathbf{E} = Re[\hat{E}_z \mathbf{i_z} \exp(j\omega t)]$ leads to the Helmholtz equation for $\hat{E}_z$

$$\boxed{\left(\frac{\partial^2}{\partial x^2} + \frac{\partial^2}{\partial y^2}\right)\hat{E}_z + \omega^2 \mu\epsilon \hat{E}_z = 0} \tag{33}$$

In retrospect, we see that the TE field relations are obtained from those for the TM fields by replacing $\mathbf{H} \rightarrow -\mathbf{E}$, $\mathbf{E} \rightarrow \mathbf{H}$, $\epsilon \rightarrow \mu$ and $\mu \rightarrow \epsilon$. This could have been expected, because in the free space regions to either side of the source sheet, Maxwell's equations are replicated by such an exchange of variables. The discussion of product solutions to the Helmholtz equation, given following (9), is equally applicable here.

**Example 12.6.2.** Traveling-Wave TE Fields

This example has two objectives. One is to illustrate the TE fields, while the other is to provide further insights into the nature of electrodynamic fields that are periodic in time and in one space dimension. In Example 12.6.1, these fields were induced by a *standing wave* of surface sources. Here the source takes the form of *a wave traveling in the x direction.*

$$K_z = Re\hat{K}_o e^{j(\omega t - k_x x)} \tag{34}$$

Again, the frequency of the source current, $\omega$, and its spatial dependence, $\exp(-jk_x x)$, are prescribed. The traveling-wave $x, t$ dependence of the source suggests that solutions take the form of (17).

$$\hat{E}_z = \begin{cases} \hat{A}e^{-j\beta y}e^{-jk_x x}; & y > 0 \\ \hat{B}e^{j\beta y}e^{-jk_x x}; & y < 0 \end{cases} \tag{35}$$

Faraday's continuity condition, (12.1.16), requires that

$$\hat{E}_z^a = \hat{E}_z^b \qquad \text{at} \qquad y = 0 \tag{36}$$

and this provides the first of two conditions on the coefficients in (35).

$$\hat{A} = \hat{B} \tag{37}$$

Ampère's continuity condition, (12.1.15), further requires that

$$-(\hat{H}_x^a - \hat{H}_x^b) = \hat{K}_z \qquad \text{at} \qquad y = 0 \tag{38}$$

With $H_x$ found by substituting (35) into (29), this condition shows that

$$\hat{A} = \hat{B} = -\frac{\omega\mu\hat{K}_o}{2\beta} \tag{39}$$

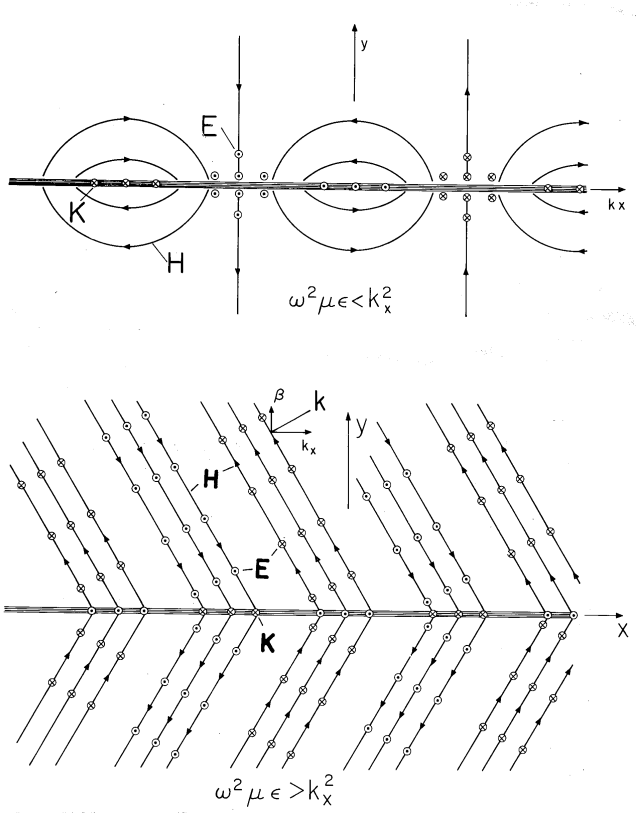


**Fig. 12.6.4** TE fields induced by traveling-wave source in the $y = 0$ plane.

With the substitution of these coefficients into (35), we have

$$E_z = Re - \frac{\omega\mu}{2\beta}\hat{K}_o e^{j(\omega t - k_x x)} \begin{cases} e^{-j\beta y}; & y > 0 \\ e^{j\beta y}; & y < 0 \end{cases} \tag{40}$$

Provided that $\beta$ is as defined by (13), these relations are valid regardless of the frequency. However, to emphasize the effect on the field when the frequency is such that $\omega^2\mu\epsilon < k_x^2$, these expressions are written for that case as

$$E_z = Re - \frac{j\omega\mu}{2|\beta|}\hat{K}_o e^{j(\omega t - k_x x)} \begin{cases} e^{-|\beta| y}; & y > 0 \\ e^{|\beta| y}; & y < 0 \end{cases} \tag{41}$$

The space time dependence of $E_z$, and $\mathbf{H}$ as found by using (40) to evaluate (29) and (30), is illustrated in Fig. 12.6.4. For $\omega^2\mu\epsilon > k_x^2$, the response to the traveling wave of surface current is waves with lines of constant amplitude given by

$$k_x x \pm k_y y = \text{constant} + \omega t \tag{42}$$

Thus, points of constant phase are lines of slope $\mp k_x/k_y$. The velocity of these lines in the $x$ direction, $\omega/k_x$, is called the phase velocity of the wave in the $x$

direction. The respective waves also have phase velocities in the $\pm y$ directions, in this case $\pm\omega/k_y$. The response to the traveling-current sheet in this high-frequency regime is a pair of uniform plane waves. Their direction of propagation is along the gradient of (42), and it is sometimes convenient to describe such plane waves by a vector wave number $\mathbf{k}$ having the direction of propagation of the planes of constant phase. The waves in the half-plane $Y > 0$ possess the $k$ vector

$$\mathbf{k} = k_x\mathbf{i_x} + k_y\mathbf{i_y} \tag{43}$$

At frequencies low enough so that $\omega^2\mu\epsilon < k_x^2$, points of constant phase lie on lines perpendicular to the $x$ axis. At a given location along the $x$ axis, the fields vary in synchronism but decay in the $\pm y$ directions. In the limit when $\omega^2\mu\epsilon \ll k_x^2$ (or $f \ll c/\lambda_x$, where $\omega \equiv 2\pi f$), the $\mathbf{H}$ fields given by (29) and (30) become the MQS fields of a spatially periodic current sheet that happens to be traveling in the $x$ direction. These "waves" are similar to those predicted by Laplace's equation except that for a given wavelength $2\pi/k_x$ in the $x$ direction, they reach out further in the $y$ direction. (A standing-wave version of this MQS field is exemplified by Prob. 8.6.9.) In recognition of the decay in the $y$ direction, they are sometimes called *nonuniform plane waves* or *evanescent waves*. Note that the frequency demarcating propagation in the $\pm y$ directions from evanescence or decay in the $\pm y$ directions is $f = c/\lambda_x$ or the frequency at which the spatial period of the imposed current sheet is equal to one wavelength for a plane wave propagating in free space.

## 12.7 ELECTRODYNAMIC FIELDS IN THE PRESENCE OF PERFECT CONDUCTORS

The superposition integral approach is directly applicable to the determination of electrodynamic fields from sources specified throughout all space. In the presence of materials, sources are induced as well as imposed. These sources cannot be specified in advance. For example, if a perfect conductor is introduced, surface currents and charges are induced on its surface in just such a way as to insure that there is neither a tangential electric field at its surface nor a magnetic flux density normal to its surface.

We have already seen how the superposition integral approach can be used to find the fields in the vicinity of perfect conductors, for EQS systems in Chap. 4 and for MQS systems in Chap. 8. Fictitious sources are located in regions outside that of interest so that they add to those from the actual sources in such a way as to satisfy the boundary conditions. The approach is usually used to provide simple analytical descriptions of fields, in which case its application is a bit of an art– but it can also be the basis for practical numerical analyses involving complex systems.

We begin with a reminder of the boundary conditions that represent the influence of the sources induced on the surface of a perfect conductor. Such a conductor is defined as one in which $\mathbf{E} \to 0$ because $\sigma \to \infty$. Because the tangential electric field must be continuous across the boundary, it follows from Faraday's continuity condition that just outside the surface of the perfect conductor (having the unit normal $\mathbf{n}$)

$$\mathbf{n} \times \mathbf{E} = 0 \tag{1}$$

In Sec. 8.4, and again in Sec. 12.1, it was argued that (1) implies that the normal magnetic flux density just outside a perfectly conducting surface must be constant.

$$\frac{\partial}{\partial t}(\mathbf{n} \cdot \mu\mathbf{H}) = 0 \tag{2}$$

The physical origins and limitations of this boundary condition were one of the subjects of Chap. 10.

**Method of Images.** The symmetry considerations used to satisfy boundary conditions in Secs. 4.7 and 8.6 on certain planes of symmetry are equally applicable here, even though the fields now suffer time delays under transient conditions and phase delays in the sinusoidal steady state. We shall illustrate the method of images for an incremental dipole. It follows by superposition that the same method can be used with arbitrary source distributions.

Suppose that we wished to determine the fields associated with an electric dipole over a perfectly conducting ground plane. This dipole is the upper one of the two shown in Fig. 12.7.1. The associated electric and magnetic fields were determined in Sec. 12.2, and will be called $\mathbf{E}_p$ and $\mathbf{H}_p$, respectively. To satisfy the condition that there be no tangential electric field on the perfectly conducting plane, that plane is made one of symmetry in an equivalent configuration in which a second "image" dipole is mounted, having a direction and intensity such that at any instant, its charges are the negatives of those of the first dipole. That is, the + charge of the upper dipole is imaged by a negative charge of equal magnitude with the plane of symmetry perpendicular to and bisecting a line joining the two. The second dipole has been arranged so that at each instant in time, it produces a tangential $\mathbf{E} = \mathbf{E}_h$ that just cancels that of the first at each location on the symmetry plane. With

$$\mathbf{E} = \mathbf{E}_h + \mathbf{E}_p \tag{3}$$

we have made $\mathbf{E}$ satisfy (1) and hence (2) on the ground plane.

There are two ways of conceptualizing the "method of images." The one given here is consistent with the superposition integral point of view that is the theme of this chapter. The second takes the boundary value point of view of the next chapter. These alternative points of view are familiar from Chaps. 4 and 5 for EQS systems and from the first and second halves of Chap. 8 for MQS systems. From the boundary value point of view, in the upper half-space, $\mathbf{E}_p$ and $\mathbf{H}_p$ are particular solutions, satisfying the inhomogeneous wave equation everywhere in the volume of interest. In this region, the fields $\mathbf{E}_h$ and $\mathbf{H}_h$ due to the image dipole are then solutions to the homogeneous wave equation. Physically, they represent fields induced by sources on the perfectly conducting boundary.

To emphasize that the symmetry arguments apply regardless of the temporal details of the excitations, the fields shown in Fig. 12.7.1 are those of the electric dipole during the turn-on transient discussed in Example 12.2.1. At an arbitrary point on the ground plane, the "real" dipole produces fields that are not necessarily in the plane of the paper or perpendicular to it. Yet symmetry requires that the tangential $\mathbf{E}$ due to the sum of the fields is zero on the ground plane, and Faraday's law requires that the normal $\mathbf{H}$ is zero as well.

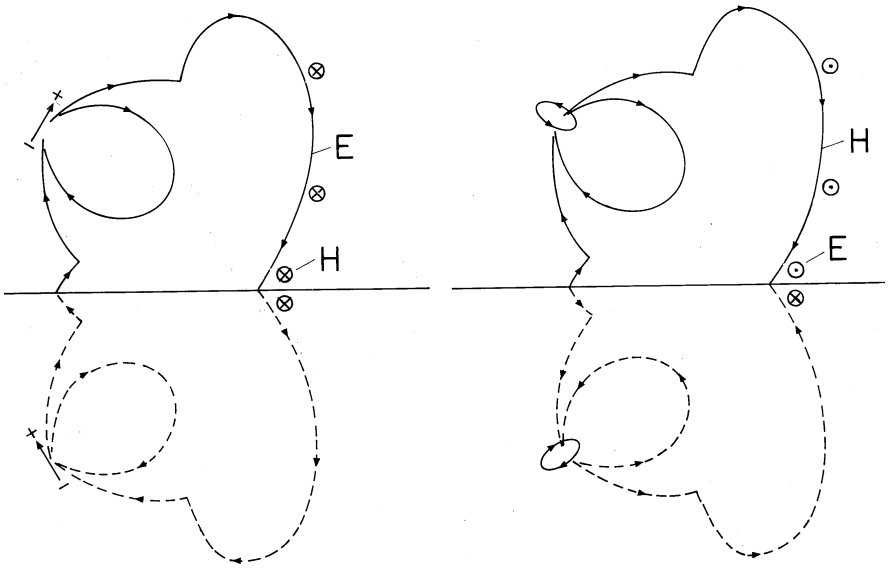


**Fig. 12.7.1** Dipoles over a ground plane together with their images: (a) electric dipole; and (b) magnetic dipole.

In the case of the magnetic dipole over a ground plane shown in Fig. 12.7.1b, finding the image dipole is easiest by nulling the magnetic flux density normal to the ground plane, rather than the electric field tangential to the ground plane. The fields shown are the dual [(12.2.33)–(12.2.34)] of those for the electric dipole turn-on transient of Example 12.2.1. If we visualize the dipole as due to magnetic charge, the image charge is now of the same sign, rather than opposite sign, as the source.

Image methods are commonly used in extending the superposition integral techniques to antenna field patterns in order to treat the effects of a ground plane and of reflectors.

**Example 12.7.1.** Ground Planes and Reflectors

**Quarter-Wave Antenna above a Ground Plane.** The center-fed wire antenna of Example 12.4.1, shown in Fig. 12.7.2a, has a plane of symmetry, $\theta = \pi/2$, on which there is no tangential electric field. Thus, provided the terminal current remains the same, the field in the upper half-space remains unaltered if a perfectly conducting ground plane is placed in this plane. The radiation electric field is therefore given by (12.4.2), (12.4.5), and (12.4.8). Note that the lower half of the wire antenna serves as an image for the top half. Whether used for AM broadcasting or as a microwave mobile antenna (on the roof of an automobile), the height is usually a quarter-wavelength. In this case, $kl = \pi$, and these relations give

$$|\hat{E}_\theta| = \frac{1}{4}\sqrt{\mu/\epsilon}\frac{I_o}{r}|\psi_o(\theta)| \tag{4}$$

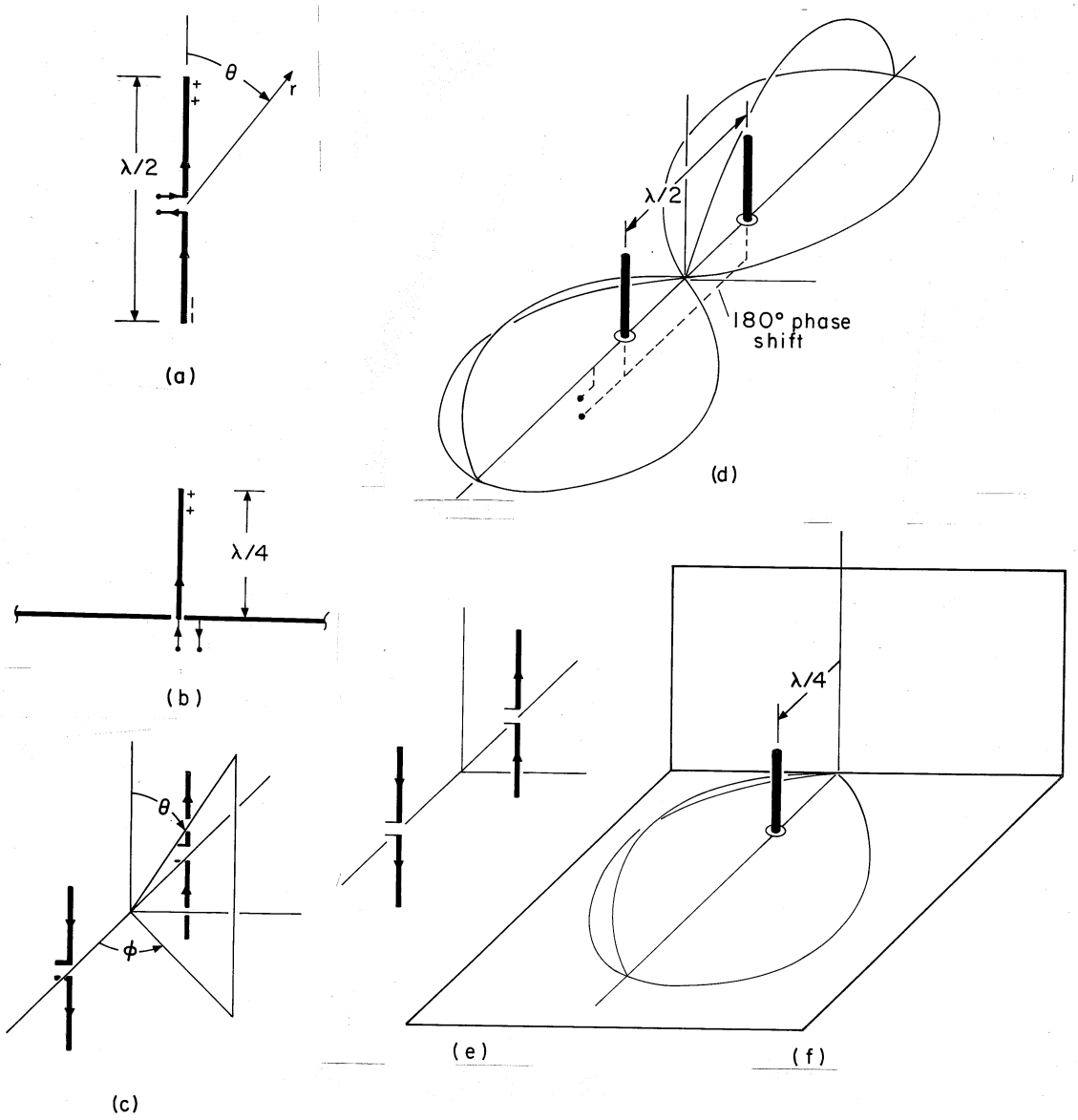


**Fig. 12.7.2** Equivalent image systems for three physical systems.

where the radiation intensity pattern is

$$\psi_o = \frac{2}{\pi} \frac{\cos\left(\frac{\pi}{2}\cos\theta\right)}{\sin\theta} \tag{5}$$

Although the radiation pattern for the quarter-wave ground plane is the same as that for the half-wave center-fed wire antenna, the radiation resistance is half as

much. This follows from the fact that the surface of integration in (12.5.9) is now a hemisphere rather than a sphere.

$$R_{\text{rad}} = \frac{1}{2\pi}\sqrt{\mu/\epsilon}\int_0^{\pi/2}\frac{\cos^2\left(\frac{\pi}{2}\cos\theta\right)}{\sin\theta}d\theta = \sqrt{\mu/\epsilon}\frac{0.61}{2\pi} \tag{6}$$

The integral can be converted to a sine integral, which is tabulated. [9] In free space, this radiation resistance is 37Ω.

**Two-Element Array over Ground Plane.** The radiation pattern from an array of elements vertical to a ground plane can be deduced using the same image arguments. The pair of center-fed half-wave elements shown in Fig. 12.7.2c have lower elements that serve as images for the quarter-wave vertical elements over a ground plane shown in Fig. 12.7.2d.

If we consider elements with a half-wave spacing that are driven 180 degrees out of phase, the array factor is given by (12.4.15) with $ka = \pi$ and $\alpha_1 - \alpha_o = \pi$. Thus, with $\psi_o$ from (5), the electric radiation field is

$$|\hat{E}_\theta| = \frac{1}{4}\sqrt{\mu/\epsilon}\frac{I_o}{r}|\psi_o(\theta)\psi_a(\theta,\phi)| \tag{7}$$

where

$$\psi_o\psi_a = \frac{4}{\pi}\cos\left[\frac{\pi}{2}(\sin\theta\cos\phi + 1)\right]\frac{\cos\left(\frac{\pi}{2}\cos\theta\right)}{\sin\theta} \tag{8}$$

The radiation pattern is proportional to the square of this function and is sketched in Fig. 12.7.2d. The field initiated by one element arrives in the far field at $\phi = 0$ and $\phi = \pi$ with a phase that reinforces that from the second element. The fields produced from the elements arrive out of phase in the "broadside" directions, and so the pattern nulls in those directions ($\phi = \pm\pi/2$).

Phased arrays of two or more verticals are often used by AM stations to provide directed broadcasting, with the ground plane preferably wet land, often with buried "radial" conductors to make the ground plane more nearly like a perfect conductor.

**Ground-Plane with Reflector.** The radiation pattern for the pair of vertical elements has no electric field tangential to a vertical plane located midway between the elements. Thus, the effect of one of the elements is equivalent to that of a reflector having a distance of a quarter-wavelength from the vertical element. This is the configuration shown in Fig. 12.7.2f.

The radiation resistance of the vertical quarter wave element with a reflector follows from (12.5.9), evaluated using (7). Now the integration is over the quarter-sphere which, together with the ground plane and the reflector plane, encloses the element at a radius of many wavelengths.

$$R_{\text{rad}} = \frac{\sqrt{\mu/\epsilon}}{\pi^2}\int_0^{\pi/2}\int_{-\pi/2}^{\pi/2}\frac{\cos^2\left[\frac{\pi}{2}(\sin\theta\cos\phi+1)\right]\cos^2\left(\frac{\pi}{2}\cos\theta\right)}{\sin\theta}d\phi d\theta \tag{9}$$

[9] It is perhaps easiest to carry out the integral numerically, as can be done with a programmable calculator. Note that the integrand is zero at $\theta = 0$.

**Demonstration 12.7.1. Ground-Planes, Phased Arrays, and Reflectors**

The experiment shown in Fig. 12.7.3 demonstrates the effect of the phase shift on the radiation pattern of the array considered in Example 12.7.1. The spacing and length of the vertical elements are 7.9 cm and 3.9 cm, respectively, which corresponds to $\lambda/2$ and $\lambda/4$ respectively at a frequency of 1.9 GHz. The ground plane consists of an aluminum sheet, with the array mounted on a section of the sheet that can be rotated. Thus, the radiation pattern in the plane $\theta = \pi/2$ can be measured by rotating the array, keeping the receiving antenna, which is many wavelengths away, fixed.

An audible tone can be used to indicate the amplitude of the received signal. To this end, the 1.9 GHz source is modulated at the desired audio frequency and detected at the receiver, amplified, and made audible through a loud speaker.

The 180 degree phase shift between the drives for the two driven elements is obtained by inserting a "line stretcher" in series with the coaxial line feeding one of the elements. By effectively lengthening the transmission line, the delay in the transmission line wave results in the desired phase delay. (Chapter 14 is devoted to the dynamics of signals propagating on such transmission lines.) The desired 180 degree phase shift is produced by rotating the array to a broadside position (the elements equidistant from the receiving antenna) and tuning the line stretcher so that the signals are nulled. With a further 90 degree rotation so that the elements are in the end-fire array position (in line with the receiving antenna), the detected signal should peak.

One vertical element can be regarded as the image for the other in a physical situation in which one element is backed at a quarter-wavelength by a reflector. This quarter-wave ground plane with a reflector is demonstrated by introducing a sheet of aluminum halfway between the original elements, as shown in Fig. 12.7.3. With the introduction of the sheet, the "image" element is shielded from the receiving antenna. Nevertheless, the detected signal should be essentially unaltered.

The experiment suggests many other interesting and practical configurations. For example, if the line stretcher is used to null the signal with the elements in end-fire array position, the elements are presumably driven in phase. Then, the signal should peak if the array is rotated 90 degrees so that it is broadside to the receiver.

**Boundaries at the Nodes of Standing Waves.** The TM fields found in Example 12.6.1 were those produced by a surface charge density taking the form of a standing wave in the $y = 0$ plane. Examination of the analytical expressions for $\mathbf{E}$, (12.6.27)–(12.6.28), and of their graphical portrayal, Fig. 12.6.3, shows that at every instant in time, $\mathbf{E}$ was normal to the planes where $k_x x = n\pi$ ($n$ any integer), whether the waves were evanescent or propagating in the $\pm y$ directions. That is, the fields have nodal planes (of no tangential $\mathbf{E}$) parallel to the $y-z$ plane. These fields would therefore remain unaltered by the introduction of thin, perfectly conducting sheets in these planes.

**Example 12.7.2.** TM Fields between Parallel Perfect Conductors

To be specific, suppose that the fields found in Example 12.6.1 are to "fit" within a region bounded by perfectly conducting surfaces in the planes $x = 0$ and $x = a$. The configuration is shown in Fig. 12.7.4. We adjust $k_x$ so that

$$k_x a = n\pi \Rightarrow k_x = \frac{n\pi}{a} \tag{10}$$

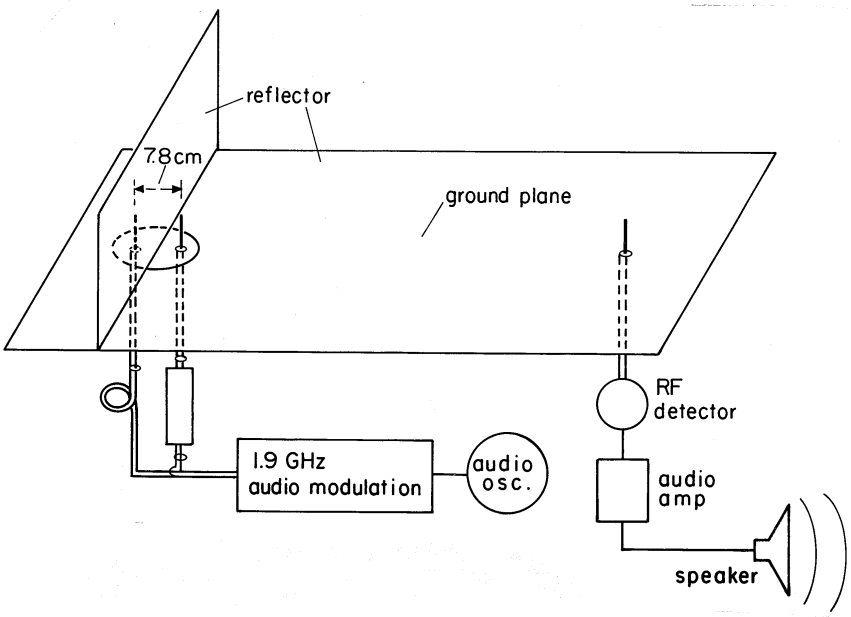


**Fig. 12.7.3** Demonstration of phase shift on radiation pattern.

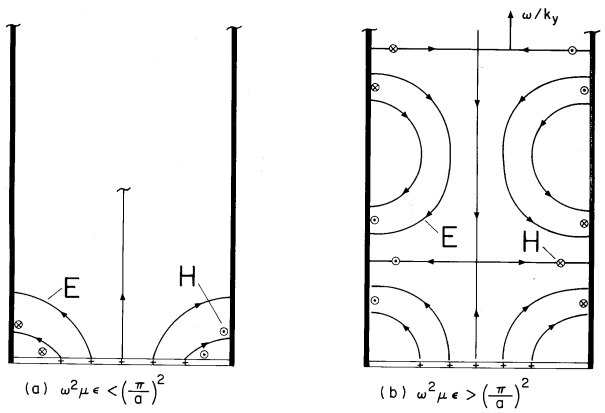


**Fig. 12.7.4** The $n = 1$ TM fields between parallel plates (a) evanescent in $y$ direction and (b) propagating in $y$ direction.

where $n$ indicates the number of half-wavelengths in the $x$ direction of the fields shown in Fig. 12.6.3 that have been made to fit between the perfect conductors. To make the fields satisfy the wave equation, $k_y$ must be given by (12.6.14) and (12.6.13). Thus, from this expression and (10), we see that for the *n-th mode* of the TM fields between the plates, the wave number in the $y$ direction is related to the frequency by

$$k_y = \beta = \begin{cases} \sqrt{\omega^2\mu\epsilon - (n\pi/a)^2}; & \omega^2\mu\epsilon > (n\pi/a)^2 \\ -j\sqrt{(n\pi/a)^2 - \omega^2\mu\epsilon}; & \omega^2\mu\epsilon < (n\pi/a)^2 \end{cases} \tag{11}$$

We shall encounter these modes and this *dispersion equation* again in Chap. 13, where waves propagating between parallel plates will be considered from the boundary value point of view. There we shall superimpose these modes and, if need be, comparable TM field modes, to satisfy arbitrary source conditions in the plane $y = 0$. The sources in the plane $y = 0$ will then represent an antenna driving a parallel plate waveguide.

The standing-wave fields of Example 12.6.1 are the superposition of two traveling waves that exactly cancel at the nodal planes to form the standing wave in the $x$ direction. To see this, observe that a standing wave, such as that for the surface charge distribution given by (12.6.18), can be written as the sum of two traveling waves.[10]

$$\sigma_s = \text{Re}\left[\hat{\sigma}_o \sin k_x x e^{j\omega t}\right] = \text{Re}\left[\frac{j\hat{\sigma}_o}{2} e^{j(\omega t - k_x x)} - \frac{j\hat{\sigma}_o}{2} e^{j(\omega t + k_x x)}\right] \tag{12}$$

By superposition, the field responses therefore must take this same form. For example, $E_y$ as given by (12.6.28) can be written as

$$E_y = \text{Re}\ \mp \frac{\hat{\sigma}_o}{4\epsilon j}\left[e^{j(\omega t \mp \beta y - k_x x)} - e^{j(\omega t \mp \beta y + k_x x)}\right] \tag{13}$$

where the upper and lower signs again refer to the regions above and below the sheet of charge density. The first term represents the response to the component of the surface current density that travels to the right while the second is the response from the component traveling to the left. The planes of constant phase for the component waves traveling to the right, as well as their respective directions of propagation, are as for the TE fields of Fig. 12.6.4. Because the traveling wave components of the standing wave have phases that advance in the $y$ direction with the same velocity, have the same wavelength in the $x$ direction and the same frequency, their electric fields in the $y$-direction exactly cancel in the planes $x = 0$ and $x = a$ at each instant in time. With this recognition, we may construct TE *modes* of the parallel plate conductor structure of Fig. 12.7.4 by superposition of two countertraveling waves, one of which was studied in Example 12.6.2.

## 12.8 SUMMARY

This chapter has been concerned with the determination of the electrodynamic fields associated with given distributions of current density $\mathbf{J}(\mathbf{r}, t)$ and charge density $\rho(\mathbf{r}, t)$. We began by extending the vector potential $\mathbf{A}$ and scalar potential $\Phi$ to situations where both the displacement current density and the magnetic induction are important. The resulting field-potential relations, the first two equations in Table 12.8.1, are familiar from quasistatics, except that $-\partial\mathbf{A}/\partial t$ is added to $-\nabla\Phi$. As defined here, with $\mathbf{A}$ and $\Phi$ related by the gauge condition of (12.1.7) in the table, the current density $\mathbf{J}$ is the source of $\mathbf{A}$, while the charge density $\rho$ is the source of

[10] $\sin u = (\exp(ju) - \exp(-ju))/2j$

**TABLE 12.8.1**

**ELECTRODYNAMIC SOURCE-POTENTIAL RELATIONS**

| | | | |
|---|---|---|---|
| $\mathbf{B} = \mu\mathbf{H} = \nabla \times \mathbf{A}$ | (12.1.1) | $\mathbf{E} = -\nabla\Phi - \dfrac{\partial \mathbf{A}}{\partial t}$ | (12.1.3) |
| $\nabla^2\mathbf{A} - \mu\epsilon\dfrac{\partial^2\mathbf{A}}{\partial t^2} = -\mu\mathbf{J}$ | (12.1.8) | $\mathbf{A} = \mu\displaystyle\int_{V'} \frac{\mathbf{J}\left(\mathbf{r}', t - \frac{\lvert\mathbf{r}-\mathbf{r}'\rvert}{c}\right)}{4\pi\lvert\mathbf{r}-\mathbf{r}'\rvert} dv'$ | (12.3.2) |
| $\nabla^2\Phi - \mu\epsilon\dfrac{\partial^2\Phi}{\partial t^2} = -\dfrac{\rho}{\epsilon}$ | (12.1.10) | $\Phi = \displaystyle\int_{V'} \frac{\rho\left(\mathbf{r}', t - \frac{\lvert\mathbf{r}-\mathbf{r}'\rvert}{c}\right)}{4\pi\epsilon\lvert\mathbf{r}-\mathbf{r}'\rvert} dv'$ | (12.3.1) |
| $\nabla\cdot\mathbf{A} + \mu\epsilon\dfrac{\partial\Phi}{\partial t} = 0$ | (12.1.7) | $\nabla\cdot\mathbf{J} + \dfrac{\partial\rho}{\partial t} = 0$ | (12.1.20) |

$\Phi$. This is evident from the finding that, written in terms of $\mathbf{A}$ and $\Phi$, Maxwell's equations imply the inhomogeneous wave equations summarized by (12.1.8) and (12.1.10) in Table 12.8.1.

Given the sources everywhere, solutions to the inhomogeneous wave equations are given by the respective superposition integrals of Table 12.8.1. As a reminder that the sources in these integrals are related, the charge conservation law, (12.1.20), is included. The relation between $\mathbf{J}$ and $\rho$ in the superposition integrals implied by charge conservation underlies the gauge relation between $\mathbf{A}$ and $\rho$, (12.1.7).

The derivation of the superposition integrals began in Sec. 12.2 with the identification of the potentials, and hence fields, associated with dipoles. Here, in remarkably simple terms, it was seen that the effect on the field at $\mathbf{r}$ of the source at $\mathbf{r}'$ is delayed by the time required for a wave to propagate through the intervening distance at the velocity of light, $c$. In the quasistatic limit, where times of interest are long compared to this delay time, the electric and magnetic dipoles considered in Sec. 12.2 are those familiar from electroquasistatics (Sec. 4.4) and magnetoquasistatics (Sec. 8.3), respectively. With the complete description of electromagnetic radiation from these dipoles, we could place the introduction to quasistatics of Sec. 3.3 on firmer ground.

For the purpose of determining the radiation pattern and radiation resistance of antennae, the radiation fields are of primary interest. For the sinusoidal steady state, Section 12.4 illustrated how the radiation fields could be superimposed to describe the radiation from given distributions of current elements representing an antenna, and how the fields from these elements could be combined to represent the radiation from an array. The elementary solutions from which these fields were constructed are those of an electric dipole, as summarized in Table 12.8.2. A similar

**TABLE 12.8.2**
**DIPOLE RADIATION FIELDS**

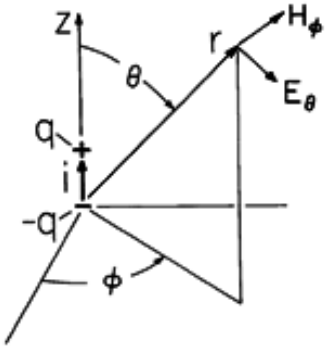


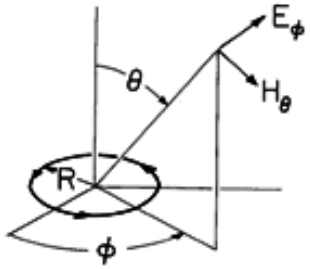


| | | | |
|---|---|---|---|
| $\hat{H}_\phi = j\frac{kd}{4\pi}\hat{i}\sin\theta\frac{e^{-jkr}}{r}$ | (12.2.23) | $\hat{E}_\phi = -\sqrt{\mu/\epsilon}\hat{H}_\theta$ | (12.2.36) |
| $k \equiv \omega/c$ | | | |
| $\hat{E}_\theta = \sqrt{\mu/\epsilon}\hat{H}_\phi$ | (12.2.24) | $\hat{H}_\theta = -\frac{k^2}{4\pi}\hat{m}\sin\theta\frac{e^{-jkr}}{r}$ | (12.2.35) |
| | | $k \equiv \omega/c$ | |

use can be made of the magnetic dipole radiation fields, which are also summarized for reference in the table.

The fields associated with planar sheet sources, the subject of Sec. 12.6, will be encountered again in the next chapter. In Sec. 12.6, the surface sources were taken as given. We found that sources having distributions that were dependent on $(x, t)$ (independent of $z$) could be classified in accordance with the fields they produced, as summarized by the figures in Table 12.8.3. The TM and TE sources and fields, respectively, are described in terms of $H_z$ and $E_z$ by the relations given in the table. In the limit $\omega^2\mu\epsilon \ll k_x^2$, these source and field cases are EQS and MQS, respectively. This condition on the frequency means that the period $2\pi/\omega$ is much longer than the time $\lambda_x/c$ for an electromagnetic wave to propagate a distance equal to a wavelength $\lambda_x = 2\pi/k_x$ in the $x$ direction.

In the form of uniform and nonuniform plane waves, the Cartesian coordinate solutions to the homogeneous wave equation for these two-dimensional fields are summarized by the last equations in Table 12.8.3. In this chapter, we have thought of $k_x$ as being imposed by the given source distribution. As the frequency is raised,

**TABLE 12.8.3**

**TWO-DIMENSIONAL ELECTRODYNAMIC FIELDS**

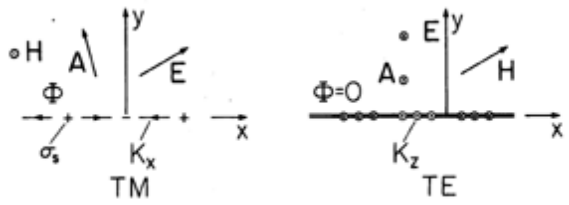


| | | | |
|---|---|---|---|
| $\left(\frac{\partial^2}{\partial x^2}+\frac{\partial^2}{\partial y^2}\right)\hat{H}_z+\omega^2\mu\epsilon\hat{H}_z=0$ | (12.6.9) | $\left(\frac{\partial^2}{\partial x^2}+\frac{\partial^2}{\partial y^2}\right)\hat{E}_z+\omega^2\mu\epsilon\hat{E}_z=0$ | (12.6.33) |
| $\hat{E}_x=\frac{1}{j\omega\epsilon}\frac{\partial\hat{H}_z}{\partial y}$ | (12.6.6) | $\hat{H}_x=-\frac{1}{j\omega\mu}\frac{\partial\hat{E}_z}{\partial y}$ | (12.6.29) |
| $\hat{E}_y=\frac{-1}{j\omega\epsilon}\frac{\partial\hat{H}_z}{\partial x}$ | (12.6.7) | $\hat{H}_y=\frac{1}{j\omega\mu}\frac{\partial\hat{E}_z}{\partial x}$ | (12.6.30) |

$$\begin{bmatrix}\hat{H}_z\\ \hat{E}_z\end{bmatrix}\propto \mathrm{Re}\,e^{j(\omega t\mp\beta y-k_x x)};\qquad \beta\equiv\begin{cases}|\sqrt{\omega^2\mu\epsilon-k_x^2}|, & \omega^2\mu\epsilon>k_x^2\\ -j|\sqrt{k_x^2-\omega^2\mu\epsilon}|, & \omega^2\mu\epsilon<k_x^2\end{cases}\qquad(12.6.13)$$

with the wavelength along the $x$ direction $\lambda_x = 2\pi/k_x$ fixed, the fields at first decay in the $\pm y$ directions (are evanescent in those directions) and are in temporal synchronism with the sources. These are the EQS and MQS limits. As the frequency is raised, the fields extend further and further in the $\pm y$ directions. At the frequency $f = c/\lambda_x$, the field decay in the $\pm y$ directions gives way to propagation.

In the next chapter, these field solutions will be found fundamental to the description of fields in the presence of perfect conductors and dielectrics.

## REFERENCES

[1] H. A. Haus and P. Penfield, Jr., **Electrodynamics of Moving Media**, MIT Press, Cambridge, Mass. (1967).

[2] J. R. Melcher, **Continuum Electromechanics**, Secs. 2.8 and 2.9, MIT Press, Cambridge, Mass. (1982).

## P R O B L E M S

### 12.1 Electrodynamic Fields and Potentials

**12.1.1*** In Sec. 10.1, the electric field in an MQS system was divided into a particular part $\mathbf{E}_p$ satisfying Faraday's law, and an irrotational part $\mathbf{E}_h$. The latter was adjusted to make the sum satisfy appropriate boundary conditions. Show that in terms of $\Phi$ and $\mathbf{A}$, as defined in this section, $\mathbf{E}_p = -\partial\mathbf{A}/\partial t$ and $\mathbf{E}_h = -\nabla\Phi$, where these potentials satisfy (12.1.8) and (12.1.10) with the time derivatives neglected.

**12.1.2** In Sec. 3.3, dimensional arguments were used to show that the quasistatic limits were valid in a system having a typical length $L$ and time $\tau$ if $L/c \ll \tau$. Use similar arguments to show that the second term on the right in either (12.1.8) or (12.1.10) is negligible when this condition prevails. Note that the resulting equations are those for MQS (8.1.5) and EQS (4.2.2) systems.

### 12.2 Electrodynamic Fields of Source Singularities

**12.2.1** An electric dipole has $q(t) = 0$ for $t < 0$ and $t > T$. When $0 < t < T$, $q(t) = Q[1-\cos(2\pi t/T)]/2$. Use sketches similar to those of Figs. 12.2.5 and 12.2.6 to show the field distributions when $t < T$ and $T < t$.

**12.2.2*** Use the "interchange of variables" property of Maxwell's equations to show that the sinusoidal steady state far fields of a magnetic dipole, (12.2.35) and (12.2.36), follow directly from (12.2.23), (12.2.24), and (12.2.32).

**12.2.3*** A magnetic dipole has a moment $m(t)$ having the time dependence shown in Fig. 12.2.5a where $dq(t) \rightarrow \mu m(t)$. Show that the fields are then much as shown in Fig. 12.2.6 with $\mathbf{E} \rightarrow \mathbf{H}$, $\mathbf{H} \rightarrow -\mathbf{E}$, and $\epsilon \leftrightarrow \mu$.

### 12.4 Antenna Radiation Fields in the Sinusoidal Steady State

**12.4.1** An "end-fed" antenna consists of a wire stretching between $z = 0$, where it is driven by the current $I_o\cos(\omega t - \alpha_o)$, and $z = l$. At $z = l$, it is terminated in such a resistance that the current distribution over its length is a wave traveling with the velocity of light in the $z$ direction; $i(z,t) = \mathrm{Re}\,[I_o \exp[j(\omega t - kz + \alpha_o)]]$ where $k \equiv \omega/c$.

(a) Determine the radiation pattern, $\Psi(\theta)$.

(b) For a one-wavelength antenna ($kl = 2\pi$), use a plot of $|\Psi(\theta)|$ to show that the lobes of the radiation pattern tend to be in the direction of the traveling wave.

**12.4.2*** An antenna is modeled by a distribution of incremental magnetic dipoles, as shown in Fig. P12.4.2. Define $\mathcal{M}(z)$ as a dipole moment per unit length so that for an incremental dipole located at $z'$, $\hat{m} \rightarrow \mathcal{M}(z')dz'$. Given $\mathcal{M}$, show that

$$\hat{E}_\phi = \frac{k^2 l}{4\pi}\sqrt{\mu/\epsilon}\frac{e^{-jkr}}{r}\mathcal{M}_o e^{j\alpha_o}\psi_o(\theta) \qquad (a)$$

where

$$\psi_o(\theta) \equiv \frac{\sin\theta}{l}\int \frac{\mathcal{M}(z')}{\mathcal{M}_o}e^{j(k\mathbf{r}'\cdot\mathbf{i}_\mathbf{r}-\alpha_o)}dz' \qquad (b)$$

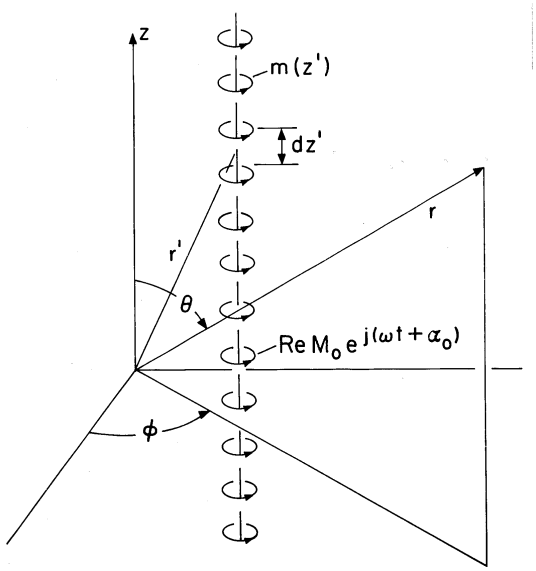


**Fig. P12.4.2**

**12.4.3** A linear distribution of magnetic dipoles, described in general in Prob. 12.4.2, is excited so that $\mathcal{M}(z') = -\mathcal{M}_o \exp(j\alpha_o)\sin\beta(z-l)/\sin\beta l$, $0 \leq z \leq l$ where $\beta$ is a given parameter (not necessarily $\omega/c$). Determine $\psi_o(\theta)$.

**12.4.4*** For the three-element array shown in Fig. P12.4.4, the spacing is $\lambda/4$.

(a) Show that the array factor is

$$\psi_a(\theta,\phi) = \left[1 + e^{j\left(\frac{\pi}{2}\cos\phi\sin\theta+\alpha_1-\alpha_o\right)} + e^{j(\pi\cos\phi\sin\theta+\alpha_2-\alpha_o)}\right] \qquad (a)$$

(b) Show that for an array of in-phase short dipoles, the "broadside" radiation intensity pattern is

$$|\psi_o|^2|\psi_a|^2 = \left[1 + 2\cos\left(\frac{\pi}{2}\cos\phi\sin\theta\right)\right]^2\sin^2\theta \qquad (b)$$

(c) Show that for an array of short dipoles differing progressively by 90 degrees so that $\alpha_1 - \alpha_o = \pi/2$ and $\alpha_2 - \alpha_o = \pi$, the end-fire radiation pattern is

$$|\psi_o|^2|\psi_a|^2 = \left\{1 + 2\cos\left[\frac{\pi}{2}(\cos\phi\sin\theta + 1)\right]\right\}^2 \sin^2\theta \qquad (c)$$

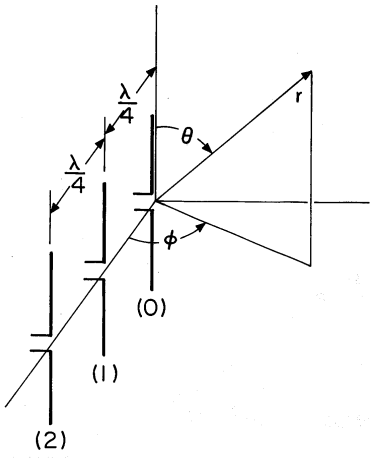


**Fig. P12.4.4**

**12.4.5** Collinear elements have the half-wave spacing and configuration shown in Fig. P12.4.5.

(a) Determine the array factor $\psi_a(\theta)$.
(b) What is the radiation pattern if the elements are "short" dipoles driven in phase?
(c) What is the gain $G(\theta)$ for the array of part (b)?

## 12.5 Complex Poynting's Theorem and Radiation Resistance

**12.5.1*** A center-fed wire antenna has a length of $3\lambda/2$. Show that its radiation resistance in free space is $104\Omega$. (The definite integral can be evaluated numerically.)

**12.5.2** The spherical coil of Example 8.5.1 is used as a magnetic dipole antenna. Its diameter is much less than a wavelength, and its equivalent circuit is an inductance $L$ in parallel with a radiation resistance $R_{\text{rad}}$. In terms of the radius $R$, number of turns $N$, and frequency $\omega$, what are $L$ and $R_{\text{rad}}$?

## 12.6 Periodic Sheet Source Fields: Uniform and Nonuniform Plane Waves

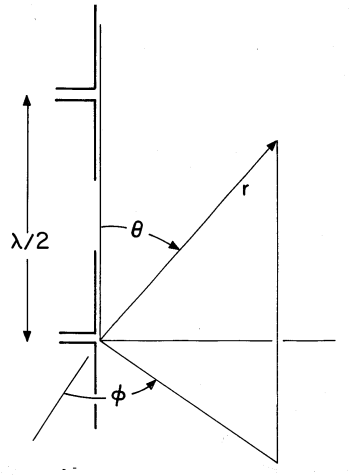


**Fig. P12.4.5**

**12.6.1*** In the plane $y = 0$, $K_z = 0$ and the surface charge density is given as the traveling wave $\sigma_s = \text{Re}\ \sigma_o \exp[j(\omega t - k_x x)] = \text{Re}\ [\sigma_o \exp(-jk_x x) \exp(j\omega t)]$, where $\sigma_o$, $\omega$, and $k_x$ are given real numbers.

(a) Show that the current density is

$$K_x = \text{Re}\ \frac{\omega\sigma_o}{k_x} e^{j(\omega t - k_x x)} = \text{Re}\left(\frac{\omega\sigma_o e^{-jk_x x}}{k_x}\right) e^{j\omega t} \qquad (a)$$

(b) Show that the fields are

$$\mathbf{H} = \mathbf{i_z} Re\big[\pm \frac{\omega\sigma_o}{2k_x} e^{\mp j\beta y} e^{j(\omega t - k_x x)}\big] \qquad (b)$$

$$\mathbf{E} = \text{Re}\left[\mathbf{i_x}\left(\frac{-\beta\sigma_o}{2\epsilon k_x} e^{\mp j\beta y}\right) + \mathbf{i_y}\big(\pm \frac{\sigma_o}{2\epsilon}\big) e^{\mp j\beta y}\right] e^{j(\omega t - k_x x)} \qquad (c)$$

where upper and lower signs, respectively, refer to the regions where $0 < y$ and $0 > y$.

(c) Sketch the field distributions at a given instant in time for $\beta$ imaginary and $\beta$ real.

**12.6.2** In the plane $y = 0$, the surface current density is a standing wave, $\mathbf{K} = \text{Re}[\mathbf{i_z} K_o$
$\sin(k_x x) \exp(j\omega t)]$, and there is no surface charge density.

(a) Determine $\mathbf{E}$ and $\mathbf{H}$.
(b) Sketch these fields at a given instant in time for $\beta$ real and $\beta$ imaginary.
(c) Show that these fields can be decomposed into waves traveling in the $\pm x$ directions with the phase velocities $\pm\omega/k_x$.

**12.6.3*** In the planes $y = \pm d/2$, shown in Fig. P12.6.3, there are surface current densities $K_z = \mathrm{Re}\,\hat{K}\exp[j(\omega t - k_x x)]$, where $\hat{K} = \hat{K}^a$ at $y = d/2$ and $\hat{K} = \hat{K}^b$ at $y = -d/2$. The surface charge density is zero in each plane.

(a) Show that

$$E_z = \mathrm{Re}\,\frac{-\omega\mu}{2\beta}\left\{\hat{K}^a\begin{bmatrix}\exp\left[-j\beta\left(y-\frac{d}{2}\right)\right]\\ \exp\left[j\beta\left(y-\frac{d}{2}\right)\right]\\ \exp\left[j\beta\left(y-\frac{d}{2}\right)\right]\end{bmatrix}+\hat{K}^b\begin{bmatrix}\exp\left[-j\beta\left(y+\frac{d}{2}\right)\right]\\ \exp\left[-j\beta\left(y+\frac{d}{2}\right)\right]\\ \exp\left[j\beta\left(y+\frac{d}{2}\right)\right]\end{bmatrix}\right\}e^{j(\omega t-k_x x)}\quad\begin{matrix};\quad \frac{d}{2}<y\\ ;\quad -\frac{d}{2}<y<\frac{d}{2}\\ ;\quad y<-\frac{d}{2}\end{matrix}\qquad (a)$$

(b) Show that if $\hat{K}^b = -\hat{K}^a\exp(-j\beta d)$, the fields cancel in region (b) where $(y < -d/2)$, so that the combined radiation is unidirectional.

(c) Show that under this condition, the field in the region $y > d/2$ is

$$E_z = \mathrm{Re}\,\frac{-\omega\mu j}{\beta}\hat{K}^a e^{-j\beta d}(\sin\beta d)e^{j\left[\omega t-\beta\left(y-\frac{d}{2}\right)-k_x x\right]};\qquad \frac{d}{2}<y \qquad (b)$$

(d) With the structure used to impose the surface currents such that $k_x$ is fixed, show that to maximize the wave radiated in region (a), the frequency should be

$$\omega = \frac{1}{\sqrt{\mu\epsilon}}\sqrt{k_x^2+\left[\frac{(2n+1)\pi}{2d}\right]^2} \qquad (c)$$

and that under this condition, the direction of the radiated wave is $\mathbf{k} = k_x\mathbf{i_x} + [(2n+1)\pi/2d]\mathbf{i_y}$ where $n = 0, 1, 2, \ldots$.

**12.6.4** Surface charges in the planes $y = \pm d/2$ shown in Fig. P12.6.3 have the densities $\sigma_s = \mathrm{Re}\,\hat{\sigma}\exp[j(\omega t - k_x x)]$ where $\hat{\sigma} = \hat{\sigma}^a$ at $y = d/2$ and $\hat{\sigma} = \hat{\sigma}^b$ at $y = -d/2$.

(a) How should $\hat{\sigma}^a$ and $\hat{\sigma}^b$ be related to produce field cancellation in region (b)?

(b) Under this condition, what is $H_z$ in region (a)?

(c) What frequencies give a maximum $H_z$ in region (a), and what is the direction of propagation under this condition?

## 12.7 Electrodynamic Fields in the Presence of Perfect Conductors

**12.7.1*** An antenna consists of a ground plane with a $3\lambda/4$ vertical element in which a "quarter-wave stub" is used to make the current in the top half-wavelength in phase with that in the bottom quarter-wavelength. In each

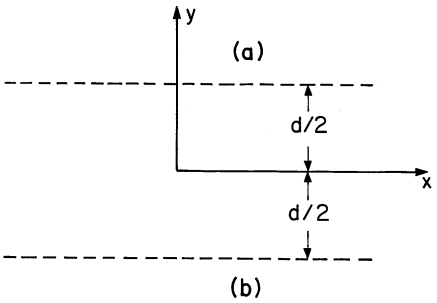


**Fig. P12.6.3**

section, the current has the sinusoidal distribution shown in Fig. P12.7.1. Show that the radiation intensity factor is

$$|\psi_o|^2|\psi_a|^2 = (2/\pi)^2|\cos[(\pi/2)\cos\theta]|^2|1 + 2\cos(\pi\cos\theta)|^2/|\sin\theta|^2$$

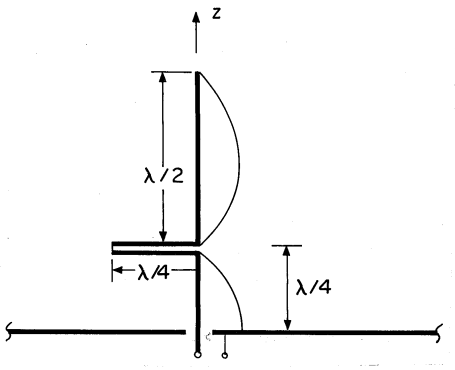


**Fig. P12.7.1**

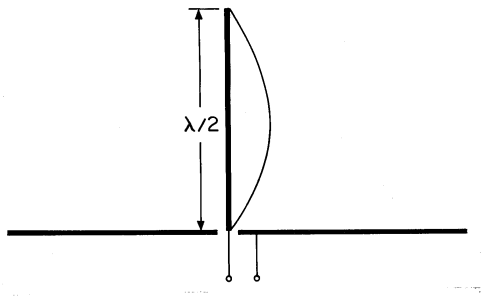


**Fig. P12.7.2**

**12.7.2** A vertical half-wave antenna with a horizontal perfectly conducting ground plane is shown in Fig. P12.7.2. What is its radiation resistance?

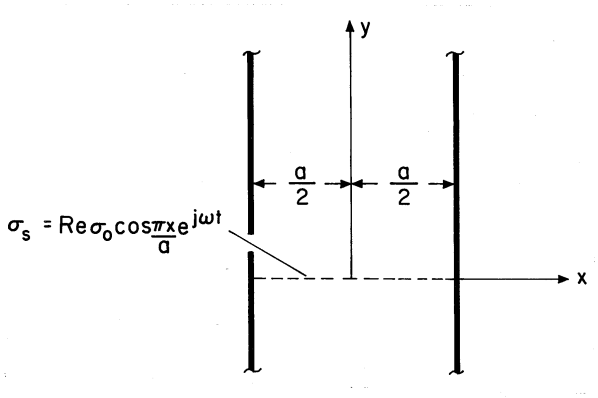


**Fig. P12.7.3**

**12.7.3** Plane parallel perfectly conducting plates in the planes $x = \pm a/2$ form the walls of a waveguide, as shown in Fig. 12.7.3. Waves in the free-space region between are excited by a sheet of surface charge density $\sigma_s = \mathrm{Re}\,\sigma_o \cos(\pi x/a)\exp(j\omega t)$ and $K_z = 0$.

(a) Find the fields in regions $0 < y$ and $0 > y$. (Guess solutions that meet both the continuity conditions at the sheet and the boundary conditions on the perfectly conducting plates.) Are they TE or TM?
(b) What are the distributions of $\sigma_s$ and $\mathbf{K}$ on the perfectly conducting plates?
(c) What is the "dispersion equation" relating $\omega$ to $\beta$?
(d) Sketch $\mathbf{E}$ and $\mathbf{H}$ for $\beta$ imaginary and real.

**12.7.4** Consider the configuration of Prob. 12.7.3, but with $\sigma_s = 0$ and $K_z = \mathrm{Re}\,\hat{K}_o \cos(\pi x/a)\exp(j\omega t)$ in the plane $y = 0$. Complete parts (a)-(d) of Prob. 12.7.3.